HEAT TRANSFER STUDY OF AIRFOIL ARRAYS IN LOW REYNOLDS NUMBER GAS FLOWS

by

Prateek Shrestha

A thesis submitted to Graduate Faculty of
Auburn University
in partial fulfillment of the
requirements for the Degree of
Master of Science

Auburn, Alabama

December 12, 2020

Keywords: heat transfer application, heat sink, airfoils in crossflow, pin-fin heat sinks

Approved by
Daniel K. Harris, Chair, Associate Professor of Mechanical Engineering
Roy W. Knight, Associate Professor of Mechanical Engineering
Mark A. Hoffman, Assistant Professor of Mechanical Engineering

Abstract

In electronic components, pin fins arrays are commonly used to manage the thermal load. Even though several shape forms and configurations of the pin fins array are possible, cylindrical and airfoil shapes in staggered arrangements are chosen for this study to compare their heat transfer properties for Reynolds number range of 500 to 1000. A numerical investigation is started by taking a single cylinder case and moving up to 16-row staggered arrays and comparing it with available empirical correlation. For airfoil geometry, NACA 0012 has been considered in the study. The numerical methodology employed with cylinder arrays was then utilized with the airfoil array. Heat transfer characteristics of NACA airfoil for three different angles of attacks (0°, 5°, and 10°) have been observed. The effect of spanwise (S_T) and streamwise (S_L) separation in staggered arrangements for both cylindrical pin fins and NACA 0012 fins has been studied. A comparison is made based on the calculated Nusselt number. The study shows that, for the cylindrical case, numerical results are close to the empirical results, which validates the numerical analysis. The Nusselt number of cylindrical arrangements is 1.1 times higher than that of the NACA 0012 array with airfoils at a 5° angle of attack. However, the overall heat transfer rate is 1.2 times higher for the same airfoil array when the domain is identical to the cylindrical array, as more airfoils could be packed in the same domain size. Additionally, the pressure drops for airfoil arrays are 5-9 times lower than the cylindrical arrays, which denote less power required to pump the fluid.

Acknowledgement

I would like to thank Dr. Daniel K. Harris for providing me with an opportunity to work on this project. I could not have been able to complete this project without his full support and guidance.

I would like to thank Dr. Roy W. Knight for his advice on issues of numerical analysis and also for his patience and support during this course of study.

I would also like to thank Dr. Mark A. Hoffman for his support as a committee member.

Special thanks go to Krishna Khanal and Basil J. Paudel for their immense support during this project. Lastly, I would like to thank my friends and family for their moral support and for giving me strength during difficult times.

Table of Contents

List of Tables

List of Figures

Nomenclature

A_1	cross section area in the transverse plane
A_2	cross section area in the diagonal plane
A_C	cross sectional area
AOA	Angle of attack
C_1	constant for Zukauskas correlation
C_2	correction factor for Zukauskas correlation
C_L or CL	chord length of airfoil
D	diameter of cylinder
k	thermal conductivity of fluid
N	number of fins
N_L	number of rows
Nu	Nusselt number based on Re
Pr	Prandtl number evaluated at film temperature
Pr_s	Prandtl number evaluated at surface temperature of fin
Re	Reynolds number based on inlet fluid velocity
Re_{max}	Reynolds number based on maximum fluid velocity

S_D	diagonal separation of fins
S_L or SL	streamwise separation of fins
S_T or ST	spanwise separation of fins
T_i	inlet temperature of fluid
T_f	film temperature
T_s	surface temperature of fin
u_m	mean velocity of fluid
V_{max}	maximum fluid velocity

Greek Symbols

ρ	density of fluid
μ	dynamic viscosity

Chapter 1 Introduction

1.1 Thermal Management Consideration

Thermal management has many applications in different fields, such as automotive industries, data centers, aerospace industries, etc. The use of electronic devices is increasing rapidly worldwide, and technological improvement has helped in manufacturing of electronic devices that are small, compatible, efficient, and cheap. Improvement in the electronics design requires optimization of the whole design, which considers material, cost, weight, heat transfer, power output, etc. As electronic devices get more powerful and smaller, thermal management of these devices becomes necessary. Without an efficient way to dissipate the device's heat, the device's temperature would increase, causing it to fail. Over the years, various thermal management systems have been developed to address this problem, which uses different cooling techniques such as [1],

a. air cooling
b. liquid cooling
c. heat pipes
d. refrigeration cooling
e. thermoelectric cooling
f. phase change material based cooling

Among various air and liquid cooling, heat sinks are widely used in the thermal management of the electronic devices.

1.2 Heat Sink

Heat sinks are passive heat exchangers which help regulate the operating temperature of a heated device. These are a common part of electronic assembly cooling designs that use fin structures. The surface area, structure, shape, and material are parameters that affect the heat sink efficiency. Various fin shapes and structures have been developed, such as flat plate shapes and pin fin shapes. For the scope of this thesis, cylinders and NACA 0012 airfoils in crossflow are examined and compared. Heat transfer behavior for a staggered array is examined, though inline arrays may be found in many practical applications.

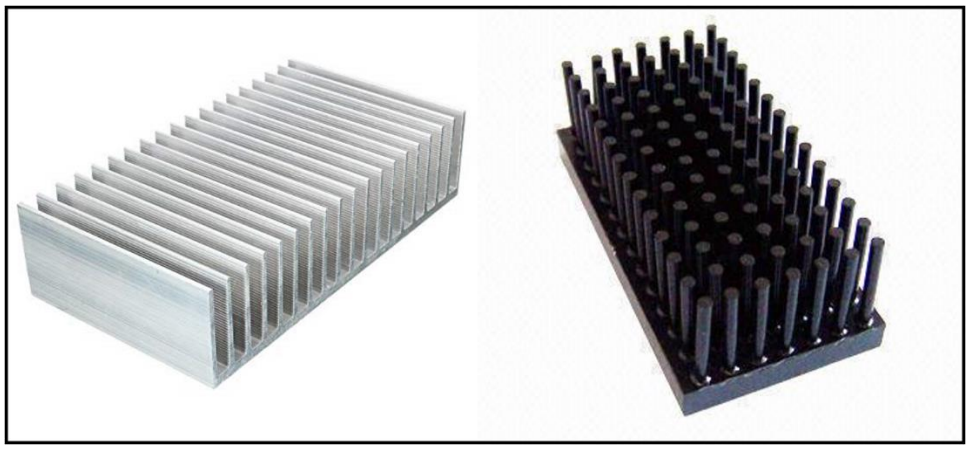

Figure 1-1 Flat plate heat sink (left) and Pin fin heat sink (right)

In electronic devices, heat sinks are used where the component's heat dissipation ability is insufficient to moderate its temperature, for example, CPUs, GPUs, and some chipsets and Ram modules. Likewise, its application extends to the cooling of gas turbines, heavy industries, and hot water boilers of the central heating system. In all applications, compact heat exchangers with high heat transfer rates are always desirable. Many studies have focused on cylindrical pin fins in inline and staggered arrangements, among which the staggered arrangement shows

higher heat transfer performance; however, it requires high pumping power than an inline array [2]. Apart from circular pin fins, other geometrical shapes can also be used in heat sinks. A NACA airfoil geometry can be used as a pin fin for laminar flows, among many geometrical shapes. As additive manufacturing technologies have reduced the difficulty in developing complex 3D geometrical models, heat sinks with airfoil arrays could be easily produced. However, much less research has been performed using airfoils as a pin fin on laminar conditions. This research is carried out to explore the prospect of airfoils as pin fins in different arrangements and compare their advantages or disadvantages to the cylindrical pin fins. Since it has been reported that airfoil pin fins produce less pressure drop [3] and hence require less pumping power, it has motivated the author to pursue this research.

1.3 Objectives

The objectives of this research are

1. To compare the simulation results of heat transfer (Nusselt number) from an array of cylinders using established empirical correlations for a Reynolds number range of 500 to 1000.
2. Perform numerical simulations to observe Nusselt number from an array of NACA 0012 airfoils in different staggered arrangements for three different angles of attack.
3. Compare Nusselt number and pressure drop for best cases of the cylindrical array and NACA 0012 airfoil array.
4. Compare the overall heat transfer rate for the cylindrical and airfoil arrays for the same domain.

5. Compare heat transfer results of the staggered airfoil array with airfoils in a meandering arrangement.

1.4 Methodology of the study

The content of the thesis is focused on comparing the heat transfer characteristics from an array of NACA 0012 airfoils in different staggered arrangements for low Reynolds number ranging from 500 to 1000. This study's methodology is shown in Figure 1-2. In Chapter 2, past research on heat transfer from pin fin arrays are presented. In Chapter 3, numerical simulations of a single cylindrical fin and staggered cylindrical fin arrangements are validated. Mesh and time-independence tests were conducted for a single cylindrical fin, and the results were compared with the Hilpert correlation. The mesh parameters used for a single cylindrical fin are then used for multiple cylinders in crossflow. Nine different staggered cylindrical pin fin arrangements were studied by changing the spanwise and streamwise spacing of the cylinders. The heat transfer results are compared with the Zukauskas correlation. The methods used to obtain numerical heat transfer results in Chapter 3 are used in Chapter 4 to model heat transfer from an array of NACA 0012 airfoils. A similar mesh independence test was conducted for a single airfoil. Then, the mesh parameters were used for multiple airfoils in a crossflow. Numerous arrangements of the airfoils can be attained by changing the angle of attack and fin spacing. Nine different staggered airfoils arrangements were similarly attained by changing the spanwise and streamwise spacing between the airfoils. Furthermore, all the arrangements were studied for three different angles of attack (0°, 5°, and 10°). Chapter 5 compares heat transfer and pressure drop from the best case cylindrical and airfoil arrays. Additionally, the overall heat transfer rate (Q) from the best arrangements was also compared with an identical domain size. Finally, among the possible arrangements, airfoils were positioned to achieve a

meandering configuration, and its heat transfer behavior was compared with a simply staggered airfoil array.

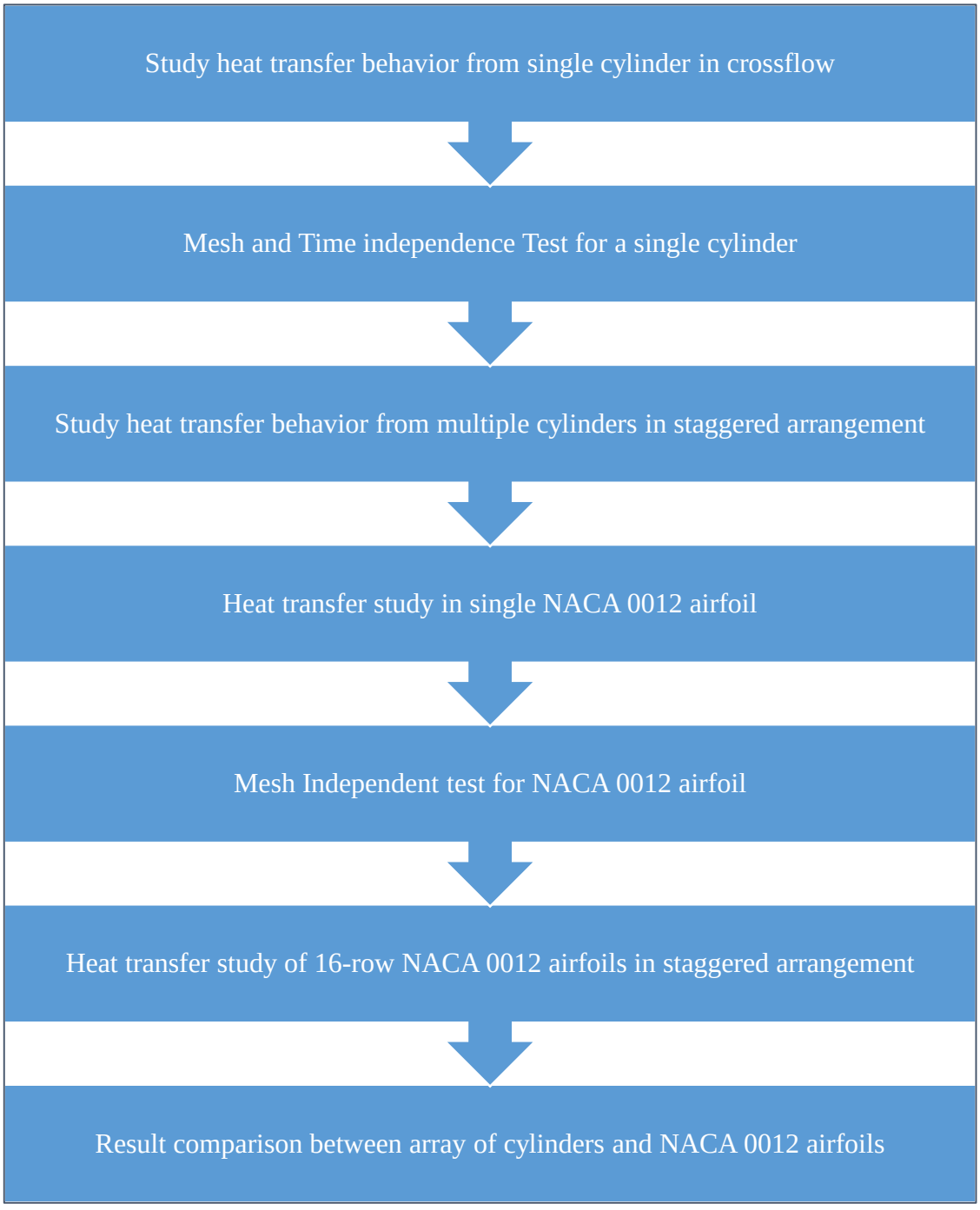

Figure 1-2 Methodology of the study

Chapter 2 Literature Review

Among various methods of electronic cooling, finned heat sinks with various geometries are widely used. One type of fin commonly used is the circular pin-fin, and many studies have been carried out to understand its heat transfer properties. While considering a cylindrical pin-fin, an infinitely long single cylinder can be considered to model the basic heat transfer behavior when cooling fluid passes across it. Various empirical correlations have been suggested for the Nusselt number of a single cylinder in crossflow [4]. A modified empirical correlation by Hilpert, which accounts for fluids of various Prandtl numbers, has been used in this thesis for Nusselt number calculation for a single cylinder in crossflow, which is given by [4]

$$\mathrm{Nu} = \mathrm{C}\,\mathrm{Re}^{\mathrm{m}}\mathrm{Pr}^{1/3} \tag{2-1}$$

Where Reynolds Number, Re, is given by

$$\mathrm{Re} = \frac{\rho \mathrm{V} \mathrm{D}}{\mu} \tag{2-2}$$

The values for constants C and m are given in Table 2-1.

Table 2-1 Constants C and m [4]

Re	C	m
0.4-4	0.989	0.330
4-40	0.911	0.385
40-4,000	0.683	0.466
4,000-40,000	0.193	0.618

In equation (2-1), all properties are evaluated at film temperature, which is the average of inlet fluid temperature and temperature of the cylinder.

However, flow characteristics and heat transfer over a surface area are different when an array of cylinders is used. Several research studies have investigated the heat transfer characteristics of cylindrical pin fin arrays with different spatial arrangements. The fins are typically arranged in either an inline or staggered configuration. The transverse or spanwise spacing (S_T) and longitudinal or streamwise spacing (S_L) are defined in Figure 2-1, which are all measured from the center of the cylinders. The diagonal spacing (S_D) is dependent upon S_T and S_L.

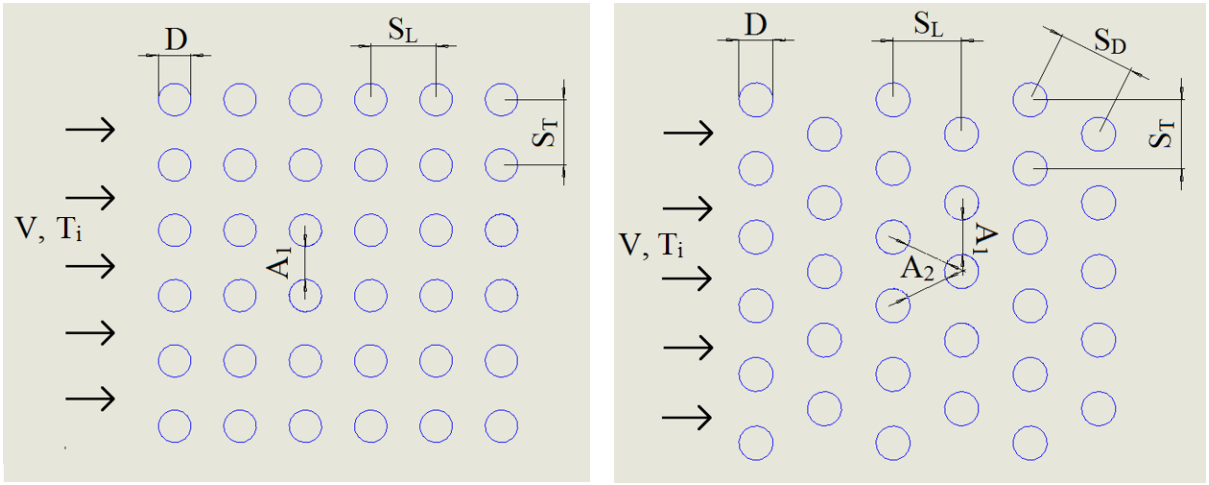

Figure 2-1 Aligned (left) and staggered (right) pin-fin arrangement

The geometry of the staggered arrangement obstructs the fluid flow and creates a winding path of fluid, which results in more heat transfer than in the inline arrangement [2][4][5]. This thesis will be focused on a staggered arrangement of cylinders. The average heat transfer coefficient for the entire bank was given by a correlation proposed by Zukauskas [6] as

$$\mathrm{Nu} = C_1 C_2 \, \mathrm{Re}_{\max}^{m} \mathrm{Pr}^{0.36} \left(\frac{\mathrm{Pr}}{\mathrm{Pr}_s}\right)^{1/4} \tag{2-3}$$

$$\begin{bmatrix} N_L \geq 20 \\ 0.7 \leq Pr \leq 500 \\ 10 \leq Re_{Dmax} \leq 2 \times 10^6 \end{bmatrix}$$

N_L is the number of cylinder rows, and C_2 is the correction factor in calculating the Nusselt number for cylinder rows less than 20. The values for C_1 and m are shown in Table 2-2, and the values for C_2 are shown in

Table 2-3**.**

The equation (2-3) uses the Reynolds number based on maximum fluid velocity, V_{max}.

$$Re_{max} = \frac{\rho V_{max} d}{\mu} \tag{2-4}$$

Where

$$V_{max} = \begin{cases} \frac{S_T}{S_T - D} V, & S_D \geq \frac{S_T + D}{2} \\ \frac{S_T}{2(S_D - D)} V, & S_D < \frac{S_T + D}{2} \end{cases} \tag{2-5}$$

$$S_D = \sqrt{S_L^2 + \left(\frac{S_T}{2}\right)^2}$$

The maximum velocity in a staggered arrangement can either occur in the transverse plane (A_1) or the diagonal plane (A_2), as shown in Figure 2-1.

The film temperature is a mean boundary layer temperature given by,

$$T_f = \frac{T_s + T_i}{2} \tag{2-6}$$

All properties in equation (2-3) are calculated at film temperature, T_f, except Pr_s, which is calculated at cylinder surface temperature T_s. The Zukauskas model has been reported to be accurate within ±15% [7].

Table 2-2 Constants for Equation (2-3) [4]

Configuration	**Re_{max}**	**C_1**	**m**
Aligned	$10\text{-}10^2$	0.80	0.40
Staggered	$10\text{-}10^2$	0.90	0.40
Aligned	$10^2\text{-}10^3$	Approximate as a single cylinder	
Staggered	$10^2\text{-}10^3$		
Aligned ($S_T/S_L > 0.7$)	$10^3\text{-}2\times10^5$	0.27	0.63
Staggered ($S_T/S_L < 2$)	$10^3\text{-}2\times10^5$	$0.35(S_T/S_L)^{0.20}$	0.60
Staggered ($S_T/S_L > 2$)	$10^3\text{-}2\times10^5$	0.40	0.60
Aligned	$2\times10^5\text{-}2\times10^6$	0.021	0.84
Staggered	$2\times10^5\text{-}2\times10^6$	0.022	0.84

Table 2-3 Correlation factor C_2 of Equation (2-3) for $N_L < 20$ [4]

N_L	1	2	3	4	5	7	10	13	16
Aligned	0.7	0.8	0.86	0.9	0.92	0.95	0.97	0.98	0.99

Staggered	0.64	0.76	0.84	0.89	0.92	0.95	0.97	0.98	0.99

Experiments performed by Sparrow et al. [2] on the inline and staggered arrangements of cylindrical pin fins reported their heat transfer and pressure drop. It was concluded that the heat transfer coefficients in the inline arrangement of cylindrical fins are lower than that of the staggered arrangement. However, the pressure drops for the staggered arrays were reported to be 50% greater than the corresponding inline arrays. Bejan [8] performed experimental, numerical, and analytical studies to determine the optimal spacing between cylinders in forced convection. It was concluded that the maximum heat transfer coefficient is achieved when the ratio between the lengths of the array to the diameter of the cylinder is taken as 6.2 for a Reynolds number range of 50-4000. Moreover, many other experiments have been conducted considering the fin spacing.

Experiments carried out by Jubran et al. [9] concluded that the optimum spacing between the fins in both spanwise and streamwise direction is 2.5 times the diameter of the cylinder in both inline and staggered arrangement of cylindrical pin fin arrays for Reynolds numbers ranging from 5,000 to 54,000. It was concluded that the maximum heat transfer is attained when the spacing between the pin fins are arranged in equilateral triangles or squares. Similarly, experiments conducted by Bilen et al. [5] in inline and staggered cylindrical pin fins arrays, with Reynolds numbers ranging from 3,700 to 30,000, showed an increase in Nusselt number with increasing Reynolds number. The maximum heat transfer occurred when the fin's streamwise spacing is kept at 2.94 with a spanwise spacing of 2.2. Khan et al. [10] developed analytical models to determine heat transfer from staggered and inline pin fin heat sinks. The

results showed that the inline arrangement has a high thermal resistance and low-pressure drop than the staggered arrangement.

Tokura et al. [11] performed experiments and presented heat transfer from a single row inline vertical array of cylinders. The average Nusselt number after the second cylinder was found to be very small when the spacing between the cylinders was narrow. The Nusselt number increased when the spacing between the cylinders was increased and reached a maximum value when the spacing was greater than five times the cylinder diameter. It was also observed that the Nusselt number of the first cylinder was almost the same as a single-cylinder when the spacing was large.

A numerical approach has also been used in investigating the heat transfer characteristics in pin fin arrays of various shapes. Sahiti et al. [3] performed a comparison of pressure drop and heat transfer on six different pin shapes. A NACA profile with a thickness of 50% of its chord length was used as one of the pin fins in the study. Their numerical investigation showed that for low Reynolds number (<1000), NACA pin fins did not show better heat transfer than other shapes of fins (cylindrical and elliptical). Dimensionless pressure drop characteristics (Euler number) were presented with a value of 0.25 for the NACA airfoil array and 0.35 for the cylindrical array, which shows that the pressure drop is lower for the airfoil array compared to the cylindrical array.

Terukazu et al. [12] used an elliptic cylinder of ratio 1:3 and determined that the heat transfer coefficient is highest for the angle of attack $\alpha = 60^0$ to 90^0 for all Reynolds numbers studied (8,000-79,000).

Li [13] performed experiments to investigate heat transfer characteristics from the staggered arrangement of short elliptical shape pin fins (Reynolds number 1,000 to 10,000) and

concluded that the heat transfer was better in elliptical pin array than cylindrical pin array. Pressure drop was also investigated in terms of dimensionless Euler number. It was found that the pressure drop of an elliptical fin array was only 58% of cylindrical fin array for a Reynolds number of 1200. Chen et al. [14] experimentally investigated the heat transfer and pressure loss characteristics of the staggered arrangement of drop-shaped and cylindrical pin fins in rectangular channels. The heat transfer from drop-shaped pin fins in the channel was found to be higher than short cylindrical pin fins (length to diameter ratio of 1) for Reynolds numbers ranging from 900-9000. However, the mean Nusselt number for both drop-shaped pin and short cylinder pin fins was very low compared to the mean Nusselt number for long cylinders proposed by Zukauskas correlation. Pressure drop in Euler number was presented, which showed that the pressure drop of drop-shaped pin fins was only 42% of that in cylindrical ones for a Reynolds number of 1200. Heat transfer characteristics with a change in spanwise and streamwise pitch of fins were also investigated.

Experiments were conducted by Uzol et al. [15] for two rows of staggered elliptical and circular pin fins. A standard elliptical fin (SEF) and NACA symmetrical airfoil fin were used. It was shown that the heat transfer from the cylindrical pin fins was 27% higher than the SEF and NACA airfoil fins array. The average pressure loss for circular fins were 44% and 52% higher than SEF and NACA airfoil fins. Wang et al. [16] performed experiments and numerical study on the array of cylindrical, elliptical, and three different drop-shaped pin fin array for a Reynolds number range of 4,800 to 8,200. It was concluded that the heat transfer was 26 % greater in circular pin fins than the drop-shaped pin fins. However, the pressure loss decreases to about 45%-55% in drop-shaped pin fins relative to circular pin fins.

A numerical investigation was done by Zhou et al. [17] to determine the thermal and hydraulic performances of plate-pin fin heat sinks with different shapes of pin fins. ANSYS CFX was

used for numerical computations using the k-ω turbulence model. Various pin fin shapes were used, ranging from cylindrical, elliptical, and NACA airfoils (thickness of 50% of its chord length). NACA airfoils showed a higher Nusselt number than cylindrical pin fins in plate-pin fin arrangement.

For higher Reynolds numbers, Jaffal et al. [18] showed that the heat transfer from drop-shaped fins was greater than circular pin fins. Wang [19] proposed a modified Hilpert correlation for heat transfer based on the experiments done on NACA 63421 airfoil arrays.

Ho et al. [20] performed experiments to determine the heat transfer performances of heat sinks with staggered arrays of NACA 0024 and NACA 4424 airfoil-shaped fins and also compared the results with heat sinks with circular and rounded rectangular fins. It was concluded that the heat transfer is greater in airfoil and rectangular fins than that of the circular pin fins. Moreover, the experiments (Reynolds number ranging from 3,400 to 24,000) were conducted on NACA 0024 airfoil fins with angles of attack ranging from 0^0 to 20^0 and concluded that the heat transfer increased with increasing angle of attack.

Table 2-4 Summary of Literature Review

Author	Re	Nu	B.C.	Analysis	Arrangement	S_T	S_L	Notes
Bilen, 2001 [5]	3700-30000	9.03-21.27	Temperature of base maintained at 45 °C	experimental	staggered cylinders	2.2D	1.96D	Re based on hydraulic diameter of flow channel; Nu based on diameter of cylinder; 3D
		8.87-21.98				2.2D	2.20D	
		9.51-25.71				2.2D	2.94D	
		8.48-23.73				2.2D	4.41D	
Khan, 2008 [10]	4000-14200	40-75	Temperature of base maintained at T_s	analytical	staggered cylinders	2.5D	1.5D	Re based on pin diameter
Jaffal, 2018 [18]	5165-41320	355-913	Constant heat flux on the base plate of heat sink	numerical (k-ε turbulence model)	staggered cylinders	2D	2D	Re and Nu based on hydraulic diameter of channel; 3D
Sahiti, 2006 [3]	193-825	31-47	Temperature of fins maintained at constant T_s	numerical (k-ε turbulence model)	staggered cylinders	Not specified explicitly		3D; Re and Nu based on hydraulic diameter of pin fin cross section
	175-740	24-46			staggered NACA profile fins			
Wang, 2012 [16]	5000-8100	51.92-59.25	Q"=10000 W/m^2	experimental	staggered cylinders	2D	3D	Re and Nu based on hydraulic diameter of channel; 3D
Ho, 2017 [20]	3400-24000	51-132	Constant input heat rate (10W)	experimental	staggered cylinders	1.25D	1.25D	3D; Re and Nu based on hydraulic diameter of channel
		70-146			staggered NACA 0024, 0° AOA	$0.5C_L$	$1C_L$	
		68-149			staggered NACA 0024, 5° AOA	$0.5\ C_L$	$1C_L$	
		69-154			staggered NACA 0024, 10° AOA	$0.5C_L$	$1C_L$	

Table 2-4 summarizes the literature review. It can be seen that most of the research has been carried out at a higher Reynolds number (Re>3000). This study is focused on the heat transfer from arrays of pin fins at a low Reynolds number range, which corresponds to low flow speed in a typical finned heat sink of a low power device. Sahiti et al. [3] numerically studied heat transfer in 3D airfoil at a 0° angle of attack for Re<1000 and reported a lower pressure drop for airfoil arrays. A lower pressure drop across a pin fin array requires a low fluid pumping power, which is much desirable because of low operating costs in practical applications. Hence, heat transfer and pressure drop are studied for NACA airfoil arrays in this study. Moreover, past studies are done for a few different spanwise and streamwise spacing of the airfoils and angles of attack [3][20]. This study extends the research by investigating heat transfer for more spanwise and streamwise spacing of the airfoils for three different angles of attack. For comparison purposes, a 2D model is used to resemble the practical application while saving computational time. Moreover, an airfoil can be aligned in different positions and angles of attack, which results in many possible configurations in an array. A meandering arrangement of airfoils is studied in this research.

Chapter 3 Cylinders in Crossflow

This chapter focuses on heat transfer from cylinders in crossflow. Section 3.1 focuses on heat transfer from cylinders using an established empirical correlation, and section 3.2 deals with observing the heat transfer behavior from numerical simulations in 2D. The diameter of the cylinder is taken as the characteristic length in the calculation of the Reynolds number. For all cases, heat transfer characteristics have been observed for four different Reynolds numbers (500, 600, 750, and 1000). Cylinders are kept at a constant temperature of 318 K, and the fluid inlet temperature is taken as 298 K. Air is taken as the working fluid for this study.

3.1 Heat transfer in cylinders from empirical correlations

3.1.1 Single-cylinder in crossflow

As discussed in Chapter 2, the Hilpert correlation for the Nusselt number of a single cylinder in crossflow is given by equation (2-1). Four different Reynolds numbers have been used for the observation of heat transfer. The calculated Nusselt number for four different Re is shown in Table 3-2. The Nusselt number is then used to calculate the average heat transfer coefficient for the single cylinder.

For all cases of cylinders, the diameter of the cylinder is taken as 10 mm. The cylinder has a constant temperature of 318 K. The fluid inlet temperature is 298 K.

Diameter of the cylinder, $D = 10$ mm

Temperature of cylinder, $T_s = 318$ K

Since fluid properties do not change significantly from temperature T_i to T_s, all fluid properties are evaluated at inlet temperature in this study, as shown in Table 3-1.

Table 3-1 Air properties at T_i

Inlet fluid temperature, T_i	298 K
Specific heat, c_p	1004.81 J/kg.K
Density, ρ	1.1855 kg/m^3
Dynamic viscosity, μ	1.836×10^{-5} kg/m.s
Thermal conductivity, k	0.02608 W/m.K
Prandtl Number, Pr	0.707

The heat transfer is observed for four Reynolds numbers for which the inlet velocity, V_i, is calculated using equation (2-2). The calculated inlet velocity is used in numerical simulations.

Table 3-2 Nusselt number and heat transfer coefficient for a single cylinder

Re	**V_i (m/s)**	**Nu (Hilpert)**	**h (W/m^2.K)**
500	0.774	11.01	28.72
600	0.929	11.99	31.27
750	1.161	13.30	34.70
1000	1.548	15.21	39.68

3.1.2 Array of cylinders in crossflow

Zukauskas [6] performed extensive experimental work and presented the correlation for cylindrical pin fins array. The correlation provides the empirical solution for staggered cylindrical pin fin arrays for a finite number of rows and a wide range of Reynolds numbers (Re ranging from 10 to $2x10^6$). Since most of the other research is carried out at higher Reynolds numbers (Re>3000), which is irrelevant to a comparison with this study, the Zukauskas correlation was selected to compare with the numerical results. The average Nusselt number for an array of cylinders can be calculated using the correlation proposed by Zukauskas, as in equation (2-3). The correlation uses a Reynolds number based on the maximum velocity of the fluid. Nine different arrangements of cylinders in a staggered position are selected for this investigation. The spanwise spacing varies from 1.75D to 2.25D, and the streamwise spacing varies from 1D to 1.5D. Parameters for the different staggered arrangement are shown in Table 3-3. The Reynolds number based on maximum velocity (V_{max}) is calculated using equation (2-4) and (2-5). The constant C_1 and m used to calculate the Nusselt Number for an array are selected from Table 2-2 for corresponding Re_{max}. The constant C_2 is selected from

Table 2-3 for 16 rows of cylinders in a staggered arrangement. The Prandtl number Pr is calculated at inlet temperature, and Pr_s is calculated at the cylinder surface temperature. However, the ratio Pr/Pr_s can be neglected for all cases as it is very close to 1.

Table 3-3 Parameters for 16-row staggered configuration of cylinders

S_T/D	S_L/D	V_{max}	C_1	m	C_2
1.75	1.00	2.33 V	0.3914	0.60	0.99
2.00	1.00	2.00 V	0.4020	0.60	0.99
2.25	1.00	1.80 V	0.4000	0.60	0.99
1.75	1.25	2.33 V	0.3744	0.60	0.99
2.00	1.25	2.00 V	0.3845	0.60	0.99
2.25	1.25	1.80 V	0.3937	0.60	0.99
1.75	1.50	2.33 V	0.3610	0.60	0.99
2.00	1.50	2.00 V	0.3707	0.60	0.99
2.25	1.50	1.80 V	0.3796	0.60	0.99

The Nusselt number calculated for four different Reynolds numbers using Zukauskas correlation can be seen in Figure 3-1. The correlation is based on Reynolds number (Re_{max}) corresponding to maximum velocity (V_{max}). However, results are presented for Reynolds numbers based on inlet fluid velocity (Re).

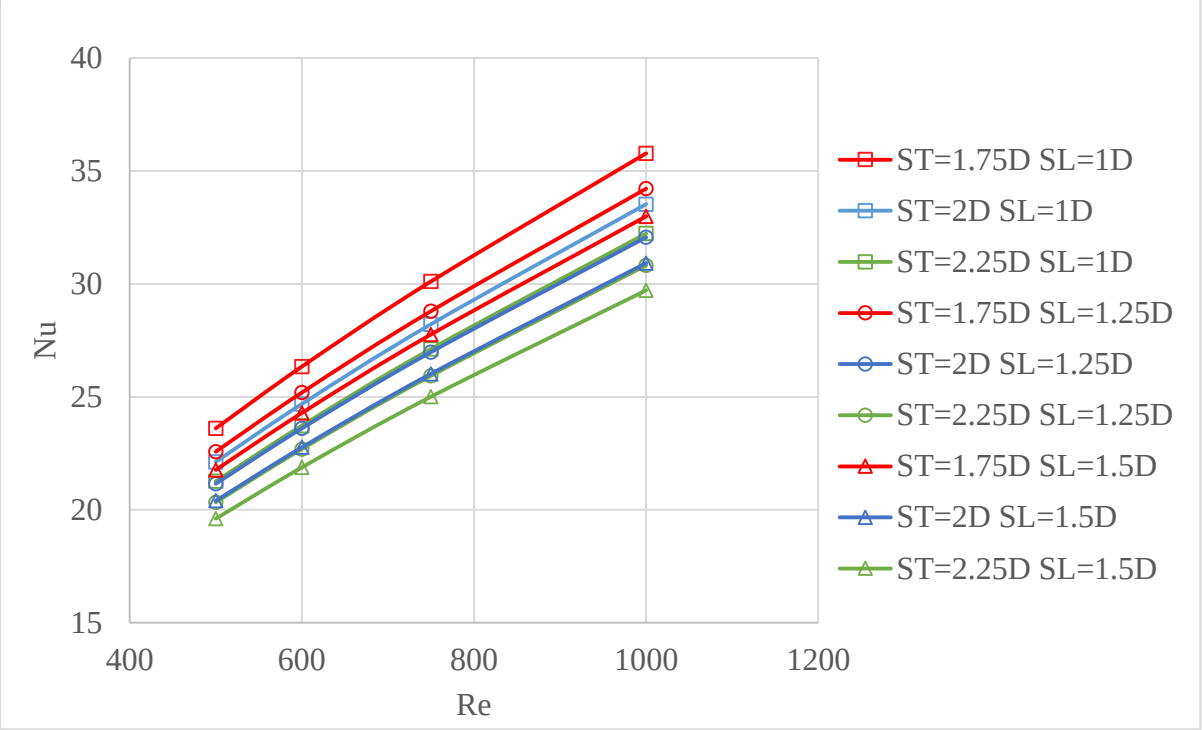

Figure 3-1 Nu (Zukauskas) for various S_T and S_L

For the nine different arrangements considered, the highest Nusselt number is obtained for the spanwise spacing of 1.75D and a streamwise spacing of 1D as per the Zukasukas correlation. These results obtained from established correlation form a baseline for comparison and validation of results obtained from numerical studies of heat transfer for the same staggered arrangements of the cylinders.

Ideally, for an infinite number of rows of fins, the temperature of the fluid approaches T_s as the fluid experiences a change in temperature as it moves through the bank of cylinders. Since the cylinders are at a constant temperature, the temperature difference (T_s-T_m), where T_m is the mean temperature of the fluid across a section, decreases exponentially as it moves through the bank [4]. Thus the total heat transfer rate is obtained by

$$Q = NhA\Delta T_{lm} \qquad (3\text{-}1)$$

Where N is the number of cylinders, h is the average heat transfer coefficient, A is the area of heat transfer for a single cylinder, and ΔT_{lm} is the logarithmic mean temperature difference given by

$$\Delta T_{lm} = \frac{(T_s - T_i) - (T_s - T_o)}{\ln\left(\frac{T_s - T_i}{T_s - T_o}\right)} \quad (3\text{-}2)$$

where T_s is the surface temperature of the cylinder, T_i is the inlet temperature of the fluid, and T_o is the outlet temperature of the fluid

Equations (3-1) and (3-2) can be used to evaluate heat transfer coefficients using the total heat transfer extracted from the numerical simulation results. Corresponding Nusselt number can then be calculated, which can be compared to the Zukauskas correlation.

3.2 Numerical simulation of heat transfer in cylinders

Numerical simulations are computed to observe the heat transfer from a single and multiple cylinders in crossflow. The obtained Nusselt number is compared with the empirical correlation from Section 3.1. The simulation is carried out in ANSYS Fluent 19.2 as an unsteady laminar flow. Mesh independence and time independence tests are conducted for a single-cylinder in crossflow. An appropriate mesh and time step are selected and then used to carry out simulations for multiple cylinders.

3.2.1 Numerical simulation of single-cylinder in crossflow

3.2.1.1 Domain geometry for a single cylinder in crossflow

The domain geometry consists of 2-D rectangular geometry with a circular cylinder, as shown in Figure 3-2. The geometry is made on the ANSYS Design Modeler.

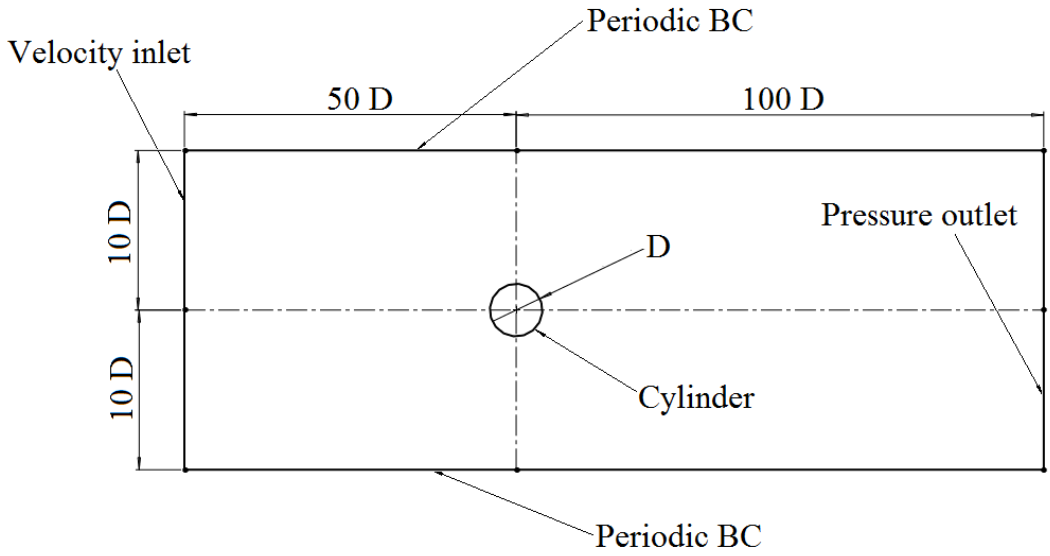

Figure 3-2 Domain geometry for a single cylinder

The domain is much greater than the cylinder diameter. The distance between the inlet plane and the cylinder is 50 times the cylinder's diameter, and the distance between the outlet and the cylinder is 100 times the diameter of the cylinder. The width of the domain is 20 times the diameter of the cylinder.

3.2.1.2 Boundary Conditions

a. Velocity Inlet: Uniform velocity is applied to the left vertical edge of the domain, as shown in Figure 3-2. The temperature of the inlet fluid is taken as 298 K.

b. Pressure Outlet: For the outlet, a pressure outlet is applied with a zero gauge pressure on the domain's right vertical plane.

c. Cylinder: A wall boundary is applied with no-slip condition. A constant wall temperature of 318 K is applied to the cylinder.

d. Periodic boundary: The top and bottom horizontal plane of the domain boundary is taken to be periodic.

3.2.1.3 Solver settings

All flows are simulated as unsteady laminar flows. The simulation is carried out until the convergence criteria are met continuously for at least 1 second. The fluid flow is taken as incompressible and the solver used is pressure-based. A second-order upwind method is used to discretize the momentum and energy equations, and a second-order implicit method is used for transient formulation. Residual values of 10^{-6} are used for the convergence criteria of x-velocity, y-velocity, and continuity, and a residual value of 10^{-9} is used for the convergence criteria of energy.

3.2.1.4 Simulation results for a single cylinder in crossflow

As the fluid approaches the front side of the cylinder, the fluid pressure rises at the stagnation point. The high pressure at the stagnation point, at the front side of the cylinder as shown in Figure 3-3, forces the fluid to move along the cylinder surface, and boundary layers develop on both sides of the cylinder. For 500<Re<1000, the flow separation occurs at 80° from the upstream stagnation point, and a periodic vortex shedding is initiated in the wake region, as shown in Figure 3-4 and Figure 3-5 [4]. The corresponding temperature field is shown in Figure 3-6.

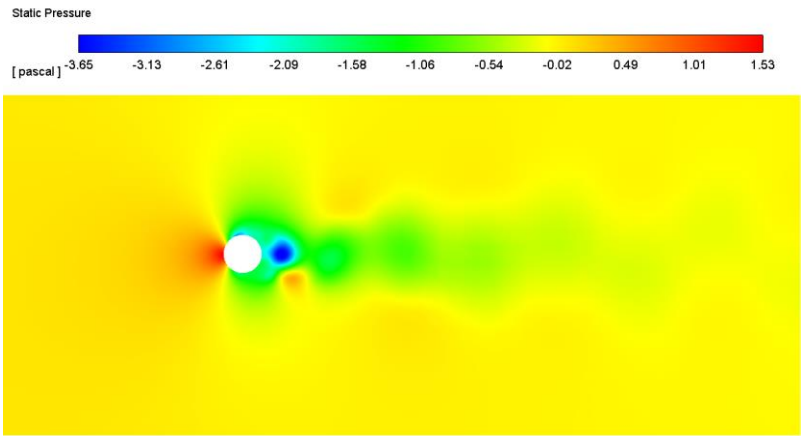

Figure 3-3 Pressure contour for single cylinder in crossflow (Re=1000, t = 1.5 s)

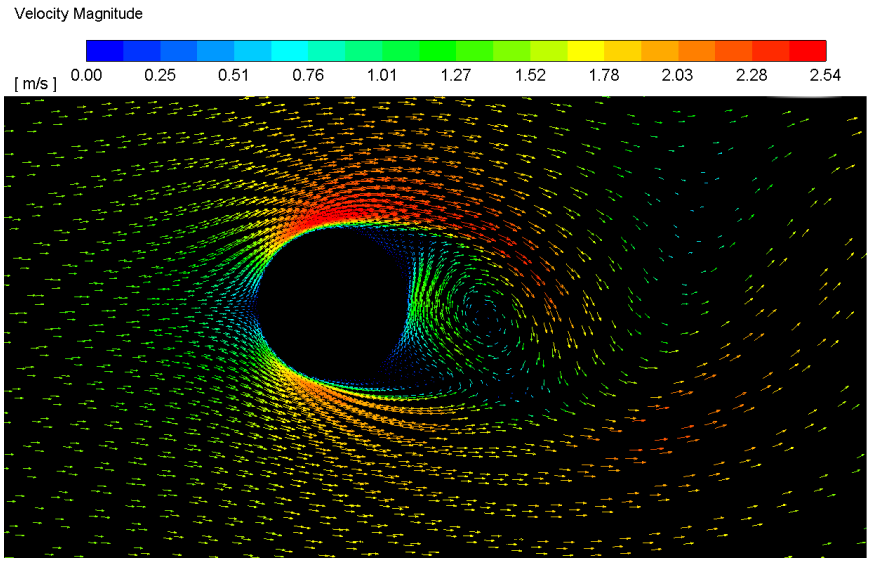

Figure 3-4 Velocity vectors for single cylinder in crossflow (Re=1000, t = 1.5 s)

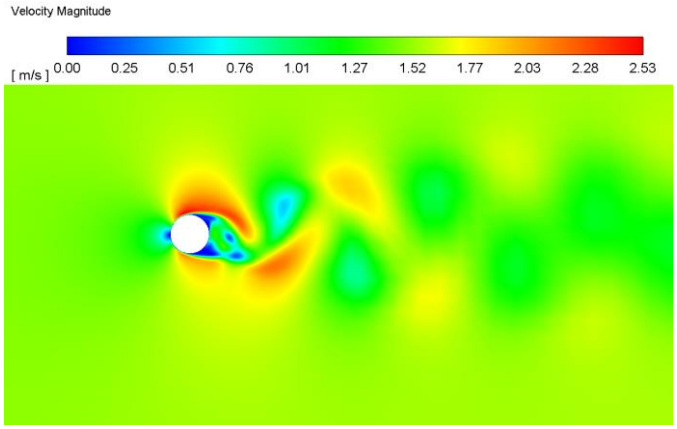

Figure 3-5 Velocity contour for single cylinder (Re=1000, t = 1.5 s)

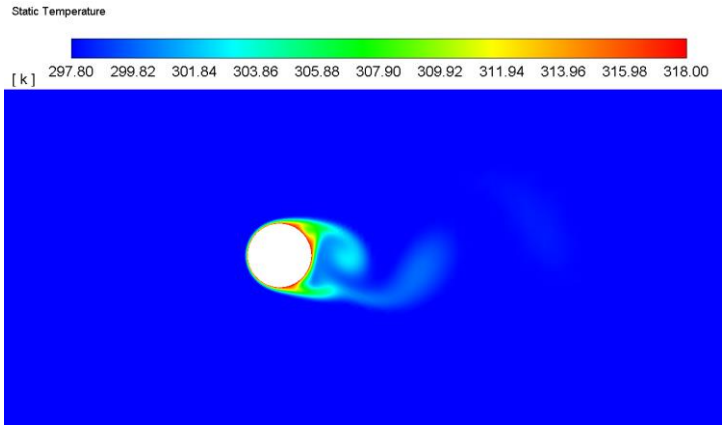

Figure 3-6 Temperature contour for single cylinder (Re=1000, t = 1.5 s)

The heat transfer rate from the cylinder is given by the equation

$$Q = hA\Delta T \tag{3-3}$$

$$Nu = \frac{hL}{k} \tag{3-4}$$

where h is the average heat transfer coefficient, Q is the heat transfer from the heated surface, A is the surface area of heat transfer, ΔT is the temperature difference (T_s-T_i), k is the thermal conductivity of the fluid, h is the average heat transfer coefficient, and L is the characteristic length which is the diameter, D, of the cylinder.

The heat transfer rate is extracted from the simulation. The transient simulation was carried out until the heat transfer rate periodically fluctuated from a mean value for at least 1 second. Then, the heat transfer rate was averaged for a time period of 1 second. The heat transfer rate is used in equation (3-3) to calculate the heat transfer coefficient. The calculated heat transfer coefficient is used in equation (3-4) to calculate the corresponding Nusselt number.

3.2.1.5 Mesh and Time independence tests

The mesh used for the simulation is a default quadrilateral mesh provided in Ansys Workbench 19.2. Inflation layers, which are thin layers of elements stacked in the direction normal to the boundary, are used around the cylinder to capture the velocity and thermal boundary layer. Different parameters shown in Table 3-4 were varied to get three different mesh geometries, as shown in Figure 3-7.

Table 3-4 Parameters for mesh generation around cylinders

Mesh	Element size (mm)	Edge sizing	Inflation layers	First layer height (mm)	Growth rate	Number for nodes	Aspect Ratio
1	6	80	35	0.1	1.2	11,325	4.08
2	5	110	50	0.05	1.1	18,197	5.76
3	4	140	80	0.025	1.05	29,974	7.83

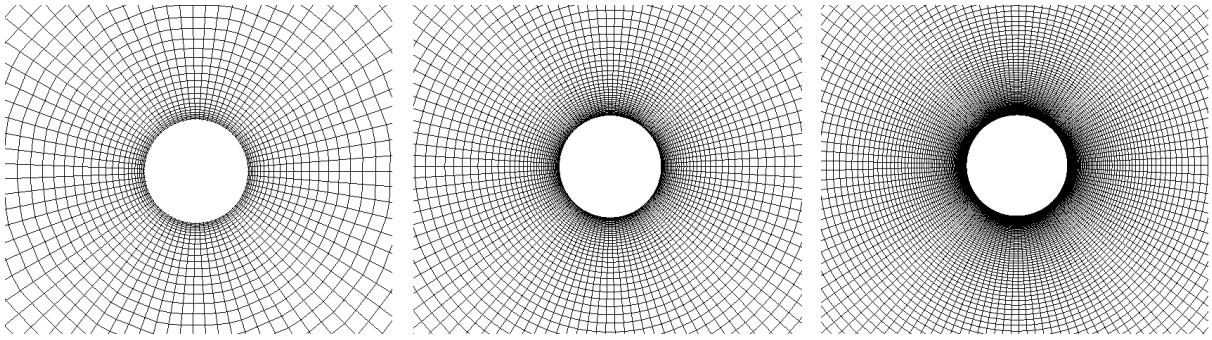

Figure 3-7 Generated mesh around cylinders

Three different time steps, 0.005, 0.0025, 0.00125 seconds, were taken for the simulation of all three meshes. A comparison of the Nusselt number using all three meshes is shown in Figure 3-8. It was found that the percentage difference between the calculated Nu was less than 2% between Mesh 1 and Mesh 2 and less than 1% between Mesh 2 and Mesh 3. There is a small difference in all three meshes. Mesh 2 was selected because the simulation time was faster than Mesh 3 and provided better results than Mesh 1.

Mesh 2 was chosen to perform a time-independence test where simulation results were compared for three timesteps. A comparison of the Nusselt number using all three time steps

and a case for Re=1000 is shown in Figure 3-9, which shows no drastic change in the average Nusselt number. It was found that the percentage difference between the calculated Nu was less than 5% between time steps 0.005 and 0.0025 seconds and less than 3% between time steps 0.0025 and 0.00125 seconds. A time step of 0.0025 seconds was selected to save computational time without compromising the accuracy.

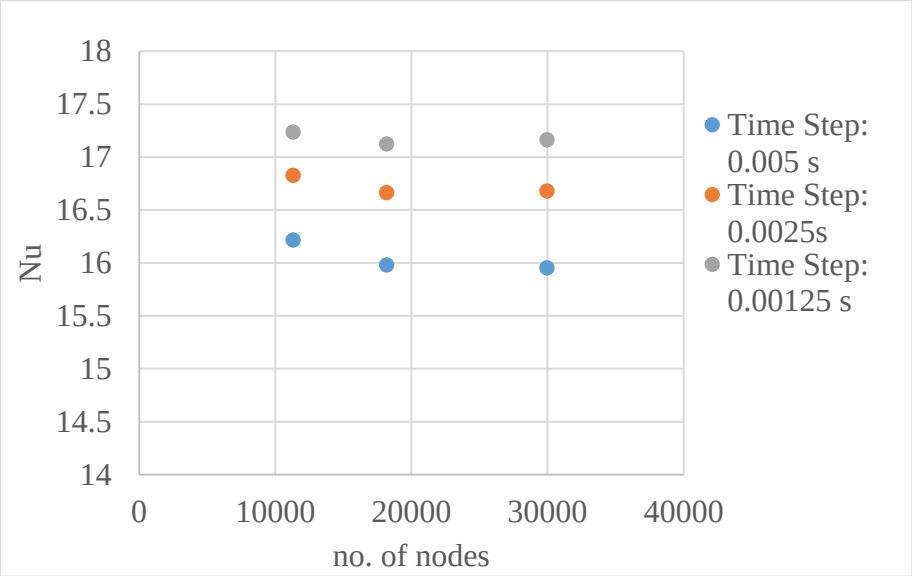

Figure 3-8 Mesh Independence test for a single cylinder (Re=1000)

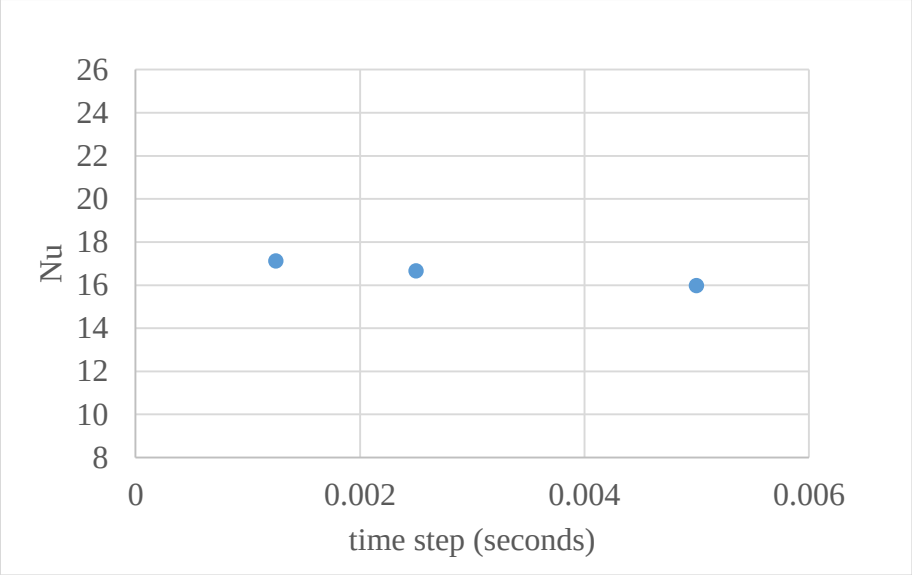

Figure 3-9 Time Independence test for a single cylinder (Re=1000)

3.2.1.6 Comparison of Nusselt number

For a single cylinder, the Nusselt number calculated from the simulation can be compared to the Hilpert correlation shown in Figure 3-10.

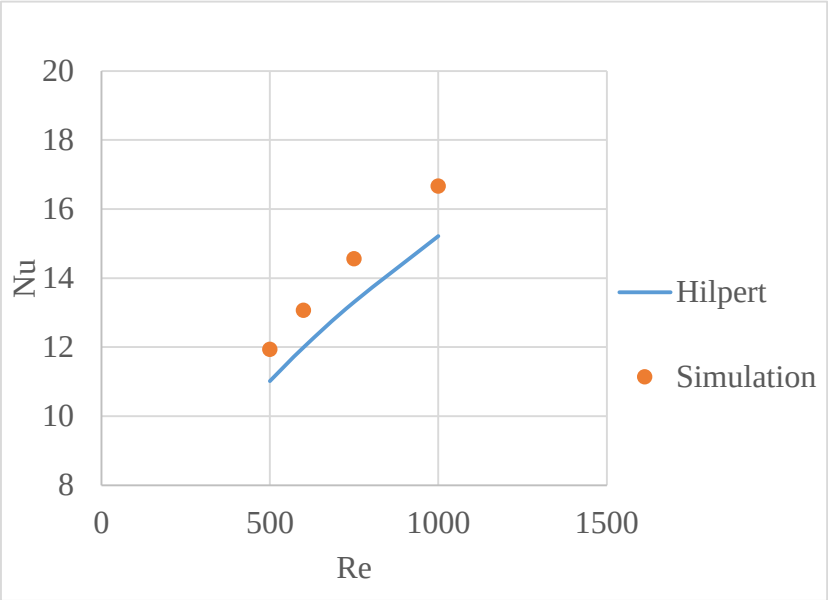

Figure 3-10 Nusselt number comparison

The percentage difference between the Nusselt number from the simulation and the correlation ranges from 8% to 10%. It can be seen that the Nusselt number is increased for higher Reynolds numbers as expected. The 2D model may not have completely depicted the experimental 3D case, but the Nusselt number from the simulation follows a similar trend line like the Hilpert correlation and within the offset of 8% to 10%.

3.2.2 Numerical simulation for two cylinders in crossflow

The heat transfer result from the simulation of a single-cylinder in crossflow is closer to that of the empirical correlation. Heat transfer from two cylinders in adjacent and inline configuration

was observed before moving on to a staggered cylinders arrangement. The arrangement of both configurations is shown in Figure 3-11.

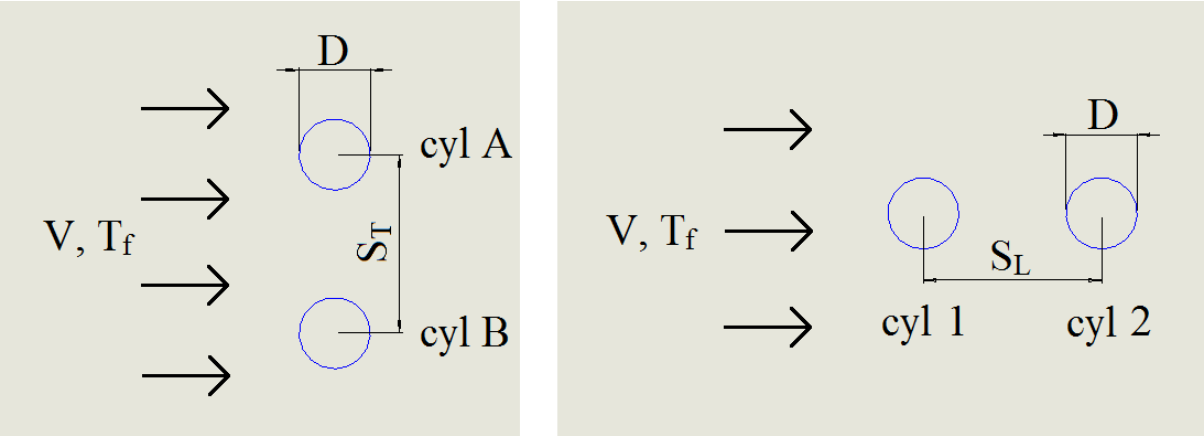

Figure 3-11 Two cylinders in adjacent (left) and inline (right) configuration

Two cylinders are separated by a spanwise pitch, S_T, in adjacent configuration, and a streamwise pitch, S_L, in an inline configuration. The domain geometry is similar to the single-cylinder in crossflow.

In an adjacent configuration, the domain width of 10 D is taken from the top cylinder to the top horizontal plane and from the bottom cylinder to the bottom horizontal plane. The total width of the domain increases as the spanwise spacing between the cylinders is increased.

However, in an inline configuration, the spacing between the first cylinder (cylinder 1) and the inlet edge is taken 50 D. Similarly, the second cylinder's distance (cylinder 2) to the outlet edge is taken as 100 D. The total length of the domain increases as the streamwise spacing between the cylinders is increased. The boundary condition and solver settings are similar as explained in Section 3.2.1

In both cases, each cylinder's heat transfer is extracted from the simulation and used in calculating the average Nusselt number for each cylinder from Equation (2-1). The spacing S_T

in adjacent and S_L in the inline arrangement is initially taken twice the cylinder's diameter and then gradually increased.

Table 3-5 Nu for two cylinders

Re	**Nu (Hilpert)**	**Nu (Simulation)**				
		Single Cylinder	**Adjacent (S_T = 2D)**		**Inline (S_L = 2D)**	
			Cylinder A	**Cylinder B**	**Cylinder 1**	**Cylinder 2**
500	11.02	11.95	12.17	12.21	9.74	4.90
600	11.99	13.10	13.34	13.39	4.90	5.60
750	13.31	14.63	14.88	14.93	11.98	6.70
1000	15.22	16.83	17.07	17.11	13.98	8.50

In an adjacent arrangement, S_T is increased from 20 mm and taken up to 120 mm. The Nusselt number of both cylinders in an adjacent arrangement should be closer to a single cylinder [4]. The Nusselt number calculated for both cylinders was found close to that of the empirical Hilpert correlation shown in Table 3-5 and Figure 3-12. As the distance between the cylinders was increased to 120 mm, the Nusselt number for both cylinders was with less than 1% different than that of a single cylinder.

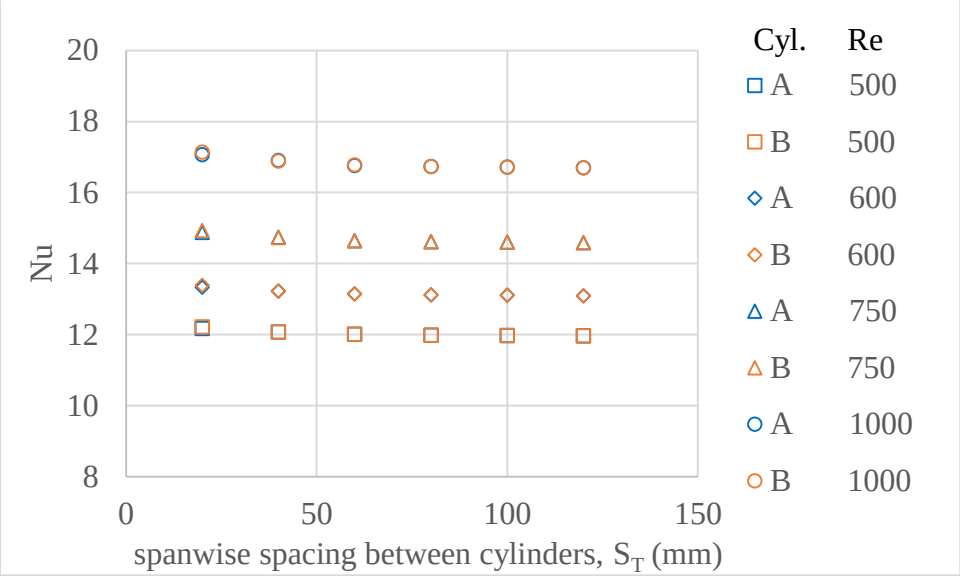

Figure 3-12 Two cylinders in an adjacent arrangement

In an inline arrangement, S_L is increased from 20 mm and taken up to 100 mm. The Nusselt number of both cylinders is shown in Figure 3-13 and Table 3-5. The heat transfer for the upstream cylinder is higher than the downstream cylinder. When the separation is increased between the cylinders, the Nusselt number of the upstream cylinder approaches that of a single cylinder as expected.

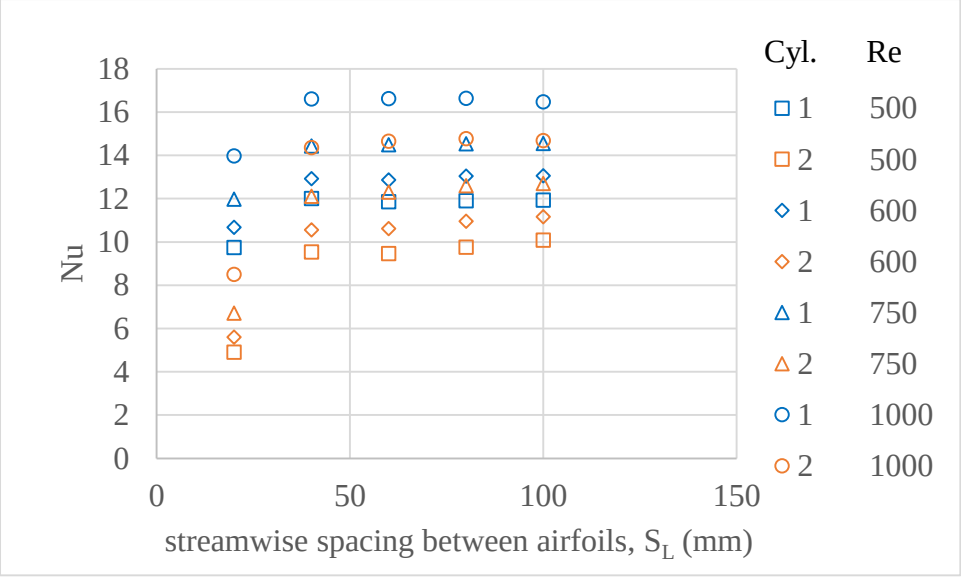

Figure 3-13 Two cylinders in inline arrangement

3.2.3 Numerical simulation for multiple rows of cylinders

Heat transfer characteristics were observed for multiple rows of cylinders in a staggered arrangement. The simulation was carried out first for the 2-row cylinder bank and then moved up to 4-row and 8-row of cylinder banks. For simplicity, the bottom and top horizontal plane of the fluid domain was reduced, as shown in Figure 3-14**,** which specifies an infinite number of cylinders in the vertical direction since the horizontal top and bottom plane is taken a periodic boundary condition. The outlet edge is 100 D distance apart from the last row of cylinders.

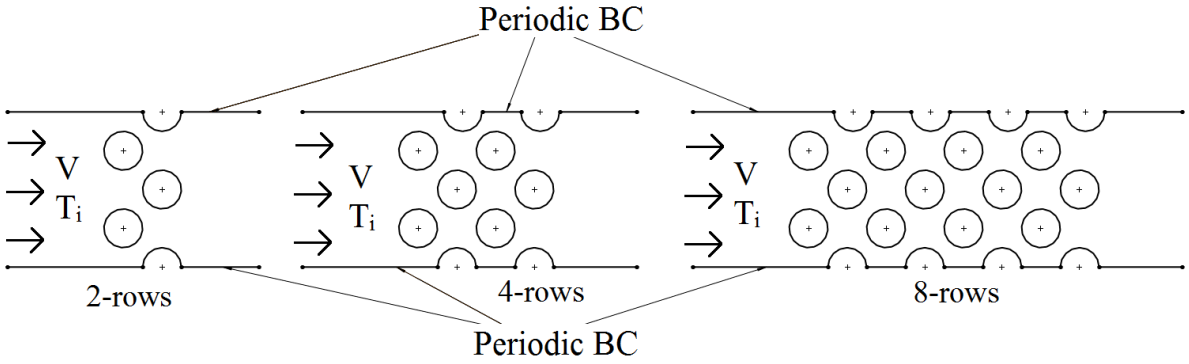

Figure 3-14 Multiple cylinders in crossflow: 2-rows, 4-rows, 8-rows

The separation S_T is 2D, and S_L is 1D with a domain width of 4D in all three cases. The domain holds a total number of 4, 8, and 16 cylinders in a 2-row, 4-row, and 8-row array for the specified arrangement. The Nusselt number of each bank of cylinders is calculated similarly to that explained for a single cylinder in Section 3.2.1.4. The average heat transfer coefficient is calculated using Equation (3-1).

For calculating mean outlet temperature T_o, the temperature data in the outlet edge of the domain was averaged by using the equation [21]

$$T_m = \frac{\int_{A_c} uTdA}{A_c u_m} \tag{3-5}$$

Where u_m is the mean velocity of fluid across a section, A_C is the cross-section area, and T and u are the temperature of fluid and x-velocity at a node along the cross-section, respectively.

The calculated Nusselt number from the simulation is compared to that found by the Zukauskas correlation and is shown in Figure 3-15, Figure 3-16, and Figure 3-17. The maximum percentage difference of Nusselt number between the correlation and the simulation is less than 6% for 2-row, 18% for 4-row, and 13% for 8-row cylinder arrangement. Given that Zukauskas correlation is within ±15% of the experimental value, it can be said the difference between simulation and the correlation results are within the acceptable range (except for the 4-row case). For the 4-row case, the error value (18%) is still close to the range (±15%). Since the numerical analysis (2D) is the simplified version of its corresponding 3D model, the simulation result and correlation are as expected and within the close range. Hence this analysis approach was used for further investigation.

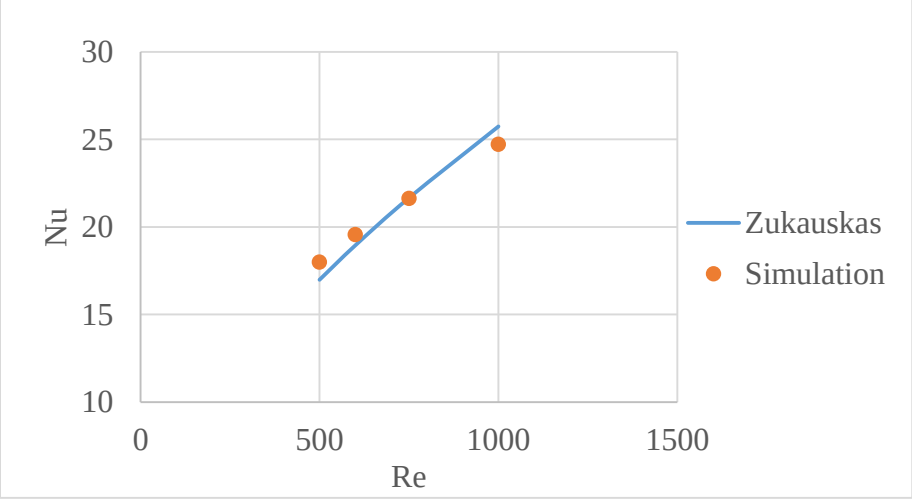

Figure 3-15 Nusselt number of 2-row cylinder array

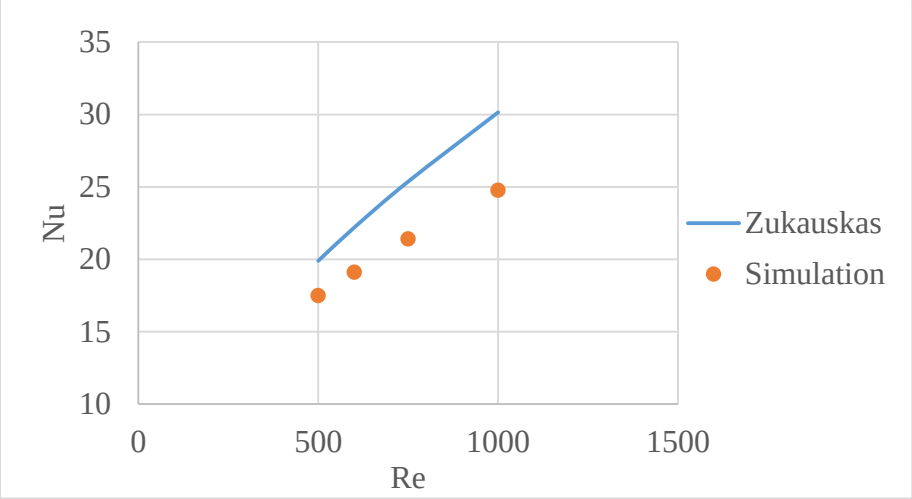

Figure 3-16 Nusselt number of 4-row cylinder array

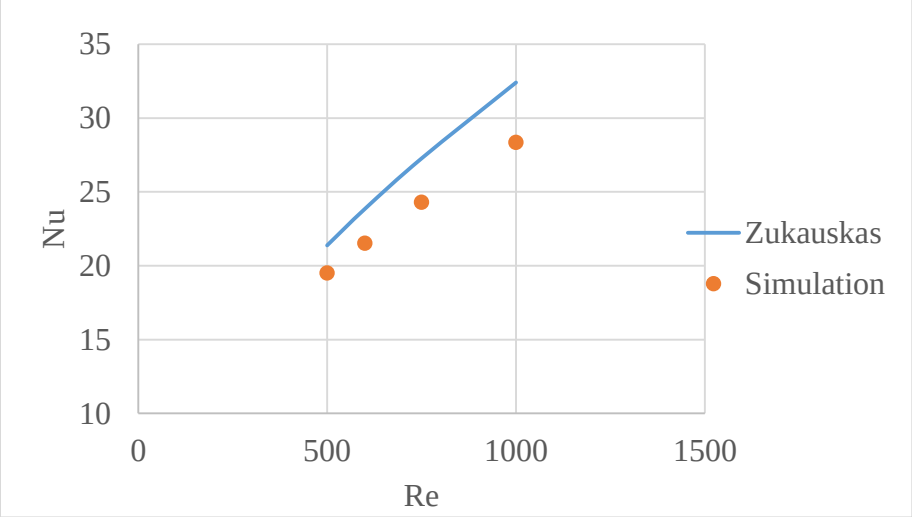

Figure 3-17 Nusselt number of 8-row cylinder array

The velocity and temperature profiles for all three cases are shown in Figure 3-18 and Figure 3-19. The mean temperature of outlet fluid increases as expected when the pin fin rows are increased.

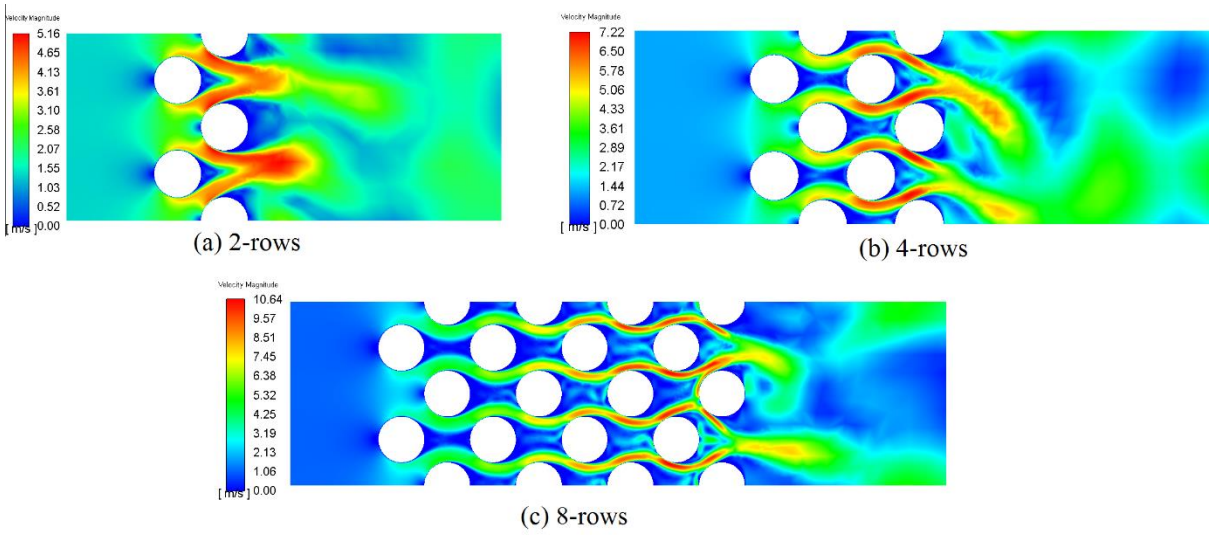

Figure 3-18 Velocity contours for Re=1000, t = 1.5 s

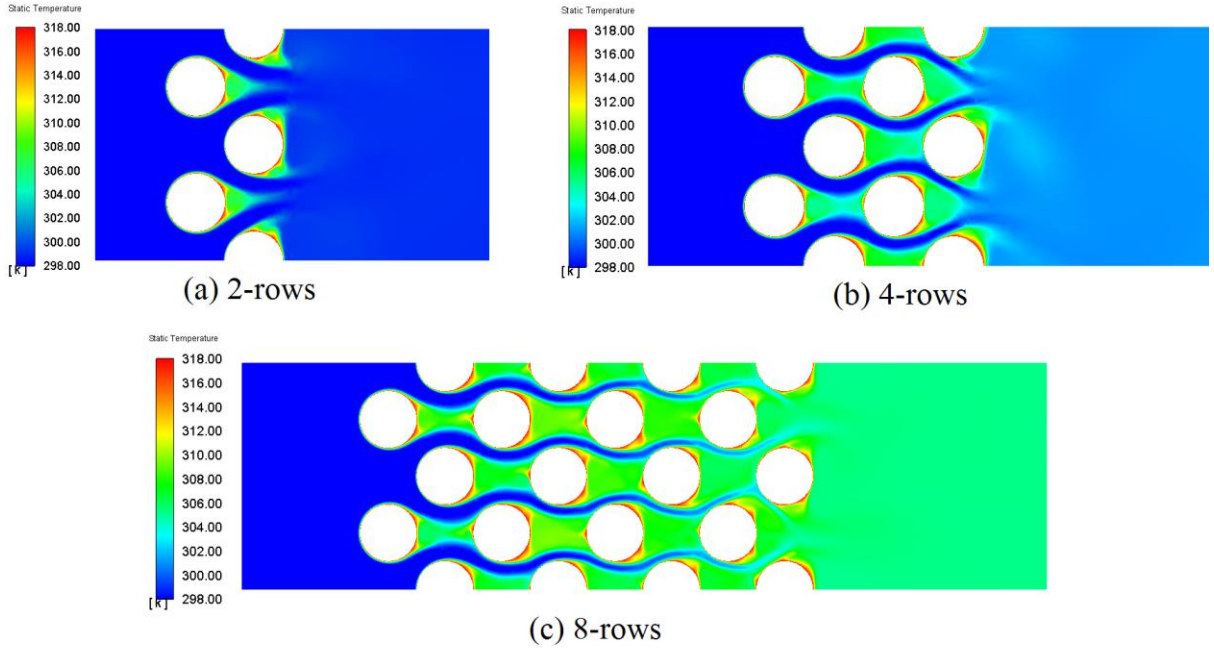

Figure 3-19 Temperature contours for Re=1000, t = 1.5 s

3.2.4 Numerical simulation for a 16-row array of cylinders

A 16-row array of cylinders, consisting of 32 cylinders, in staggered configuration was taken, and heat transfer from the array was examined and compared with the correlation provided by Zukauskas. Nine different arrangements of cylinders were taken by varying the spanwise and streamwise pitch of cylinders. As the spanwise spacing is varies, the domain's width also changes accordingly. The calculated Nusselt numbers are shown in Figure 3-20.

The maximum percentage difference between the Nusselt number from Zukauskas correlation and the simulation is less than 17%, which is well within the uncertainties (as explained in Section 3.2.3). The Nusselt number is highest for a spanwise and streamwise spacing of 1.75D and 1D, respectively, which agrees with the Zukauskas correlation results.

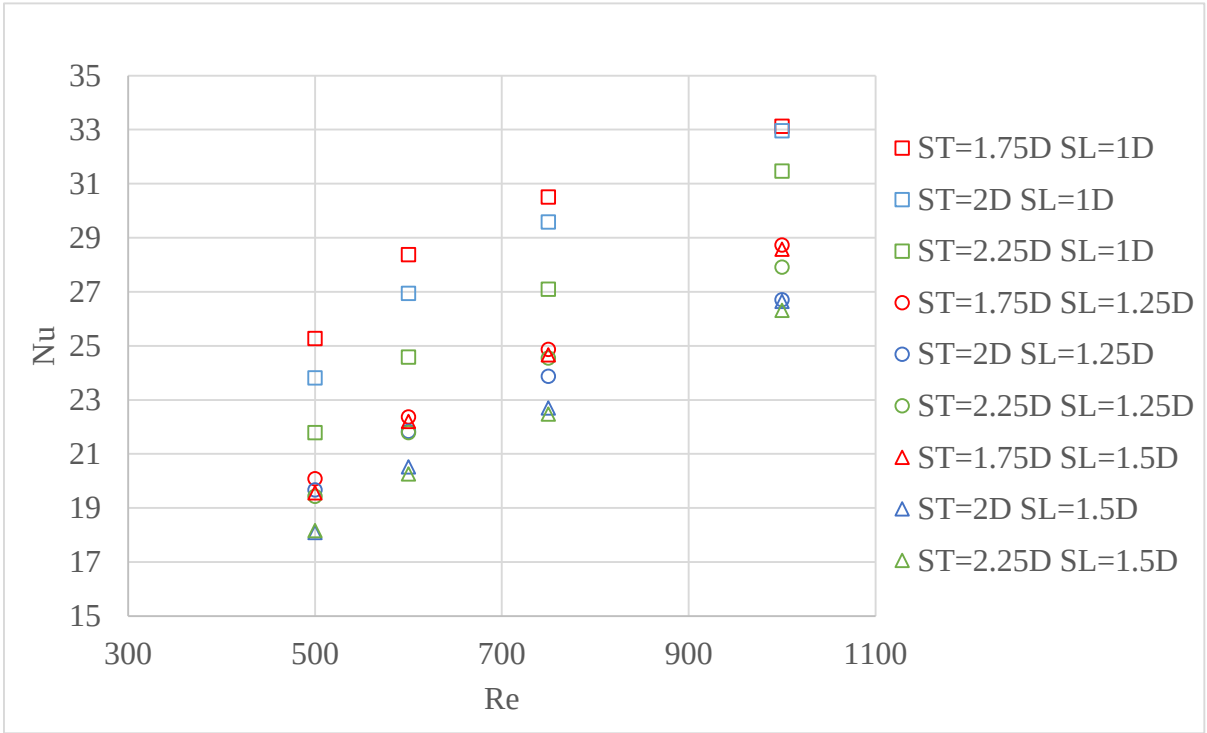

Figure 3-20 Nu (simulation) for nine different S_T and S_L

It is also observed that when the streamwise spacing is kept constant at 1D, the Nusselt number is maximum for the smallest spanwise spacing of 1.75D and decreases as the spanwise spacing is increased.

The maximum difference in Nusselt number between the numerical result and Zukauskas is 8.68% for the staggered case of S_T=1.75 D and S_L=1D, as shown in Figure 3-21. Nusselt number comparison for all nine staggered arrangement is presented in Appendix Table A- 2. The maximum difference between the Zukauskas and simulation result is observed for the arrangement of S_T=2D and S_L=1.25D for Reynolds number of 1000. The velocity, temperature, and pressure fields are shown in Figure 3-22,Figure 3-23, and Figure 3-24 for t=1.5 seconds. From Figure 3-22, the velocity is observed highest at the diagonal spacing, which agrees with the Zukauskas model. Figure 3-23 shows that as the air leaves the array, its temperature reaches around 313 K.

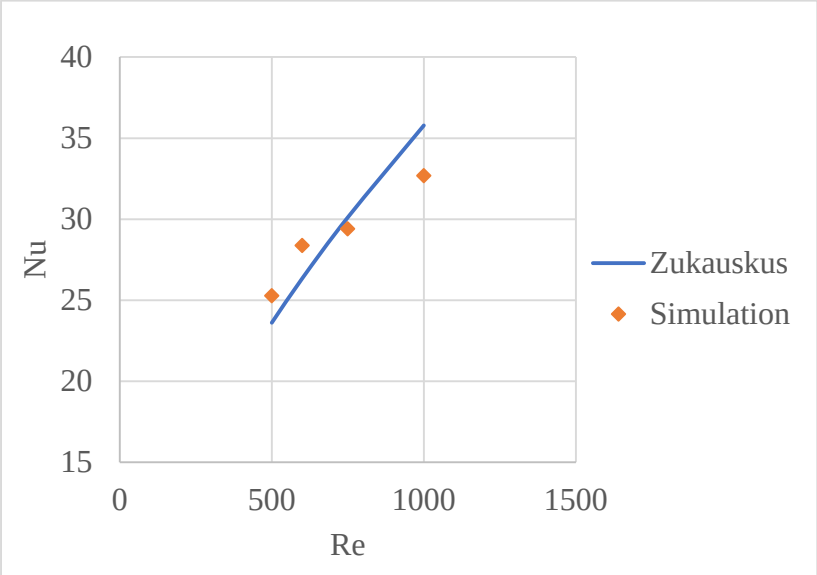

Figure 3-21 Nusselt number comparison for staggered cylinders, S_T=1.75 D and S_L=1D

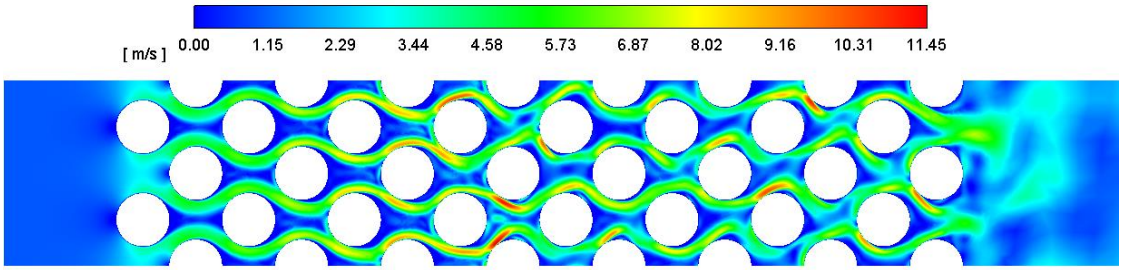

Figure 3-22 Velocity contour for S_T=1.75D, S_L=1D (Re = 1000)

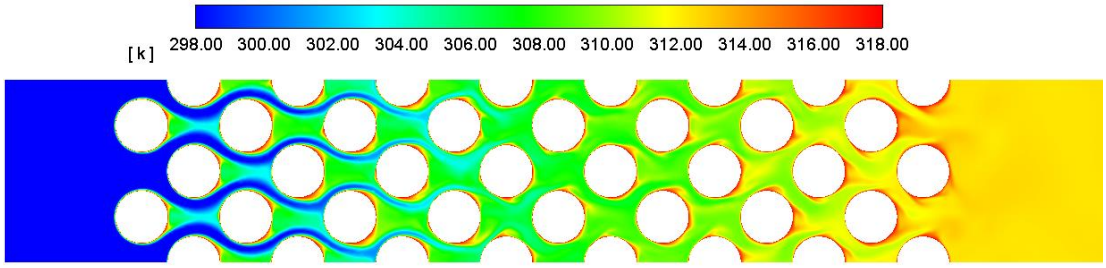

Figure 3-23 Temperature contour S_T=1.75D, S_L=1D (Re = 1000)

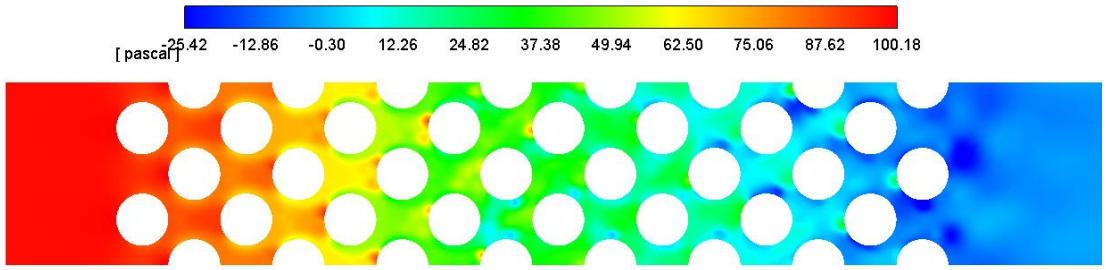

Figure 3-24 Pressure contour S_T=1.75D, S_L=1D (Re = 1000)

Chapter 4 Airfoils in crossflow

The simulation of cylindrical cases lined up close to the established correlation by Zukauskas, as discussed in the previous section. There has been less research on heat sinks with NACA airfoils as pin fins in different arrangements. Out of several NACA profiles, a simple symmetrical NACA airfoil with a thickness of 12% of its chord length (NACA 0012) was chosen for this study. Since the empirical correlation for airfoil pin fins is not available for the low Reynolds number range, heat transfer properties are compared with the cylindrical array. The Reynolds number was calculated using the chord length of the airfoil as the characteristic length. Thus, the fluid inlet velocities are the same for both cylinder and airfoil cases. For the observed Reynolds number range, the flow over the airfoil is laminar [22]. Thus, the simulations are carried out for laminar conditions with a steady-state solver, which provides time-averaged results of flow and heat transfer. The same modeling technique as in cylindrical array is adopted to investigate the heat transfer from symmetrical NACA airfoil pin fin array for nine different staggered arrangements. Furthermore, heat transfer is observed for three different angles of attack (0°, 5°, and 10°). The angle of attack of the airfoil is measured relative to the inlet fluid flow velocity direction.

4.1 Heat transfer in a single NACA 0012 airfoil in crossflow

4.1.1 Domain Geometry

A NACA 0012 airfoil of chord length 10 mm was used in all simulations which has an airfoil perimeter of 20.39 mm. The domain and boundary conditions used for a single airfoil are similar to that of the cylinder explained in Section 3.2.1 The domain size is measured from the leading edge of the airfoil, as shown in Figure 4-1. Unlike cylinders, the airfoil does not produce vortex shedding for the low Reynolds number range. Hence, a steady-state solver was

used. Residual values of 10^{-6} were used for the convergence criteria of x-velocity, y-velocity, and continuity, and a residual value of 10^{-9} is used for the convergence criteria of energy.

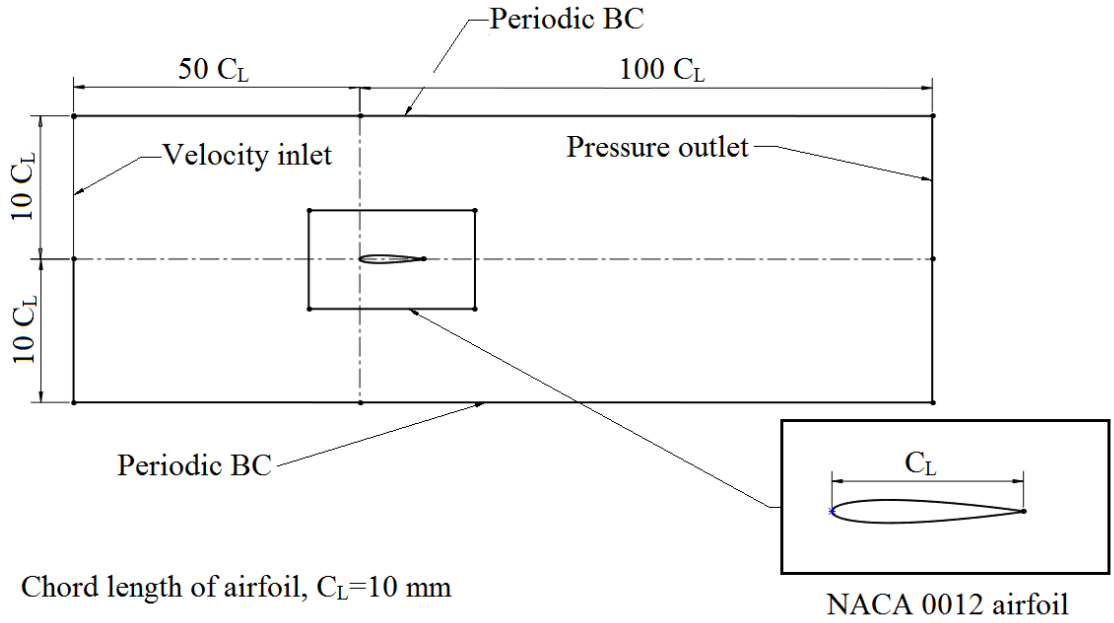

Figure 4-1 Domain geometry for a NACA 0012 airfoil

4.1.2 Mesh independence test

An unstructured quadrilateral mesh with inflation layers is used around the airfoil as shown in Figure 4-2. Different parameters such as edge sizing around the airfoil, inflation layers, the growth rate of inflation layers, and global mesh size were changed to get different meshes as shown in

Table 4-1. Elliptical projection lines were drawn around the airfoil to adjust the transition of mesh from the airfoil to the whole domain. The element size within the elliptical projections was also varied.

The Nusselt numbers for the airfoil are calculated using the heat transfer rate obtained from the simulation. The heat transfer rate was directly extracted from ANSYS Fluent. Equation (3-3) and (3-4) were used in calculating the average Nusselt number around the airfoil. The Nusselt number for airfoil is calculated using chord length.

A comparison of the Nusselt number using all three meshes is shown in Figure 4-3. It can be seen that there is no drastic change in Nusselt number even though the mesh size was made fine. It was found that the percentage difference between the calculated Nu was less than 1% in all three meshes. Mesh parameters similar to Mesh 2 were adopted for mesh generation of staggered airfoils.

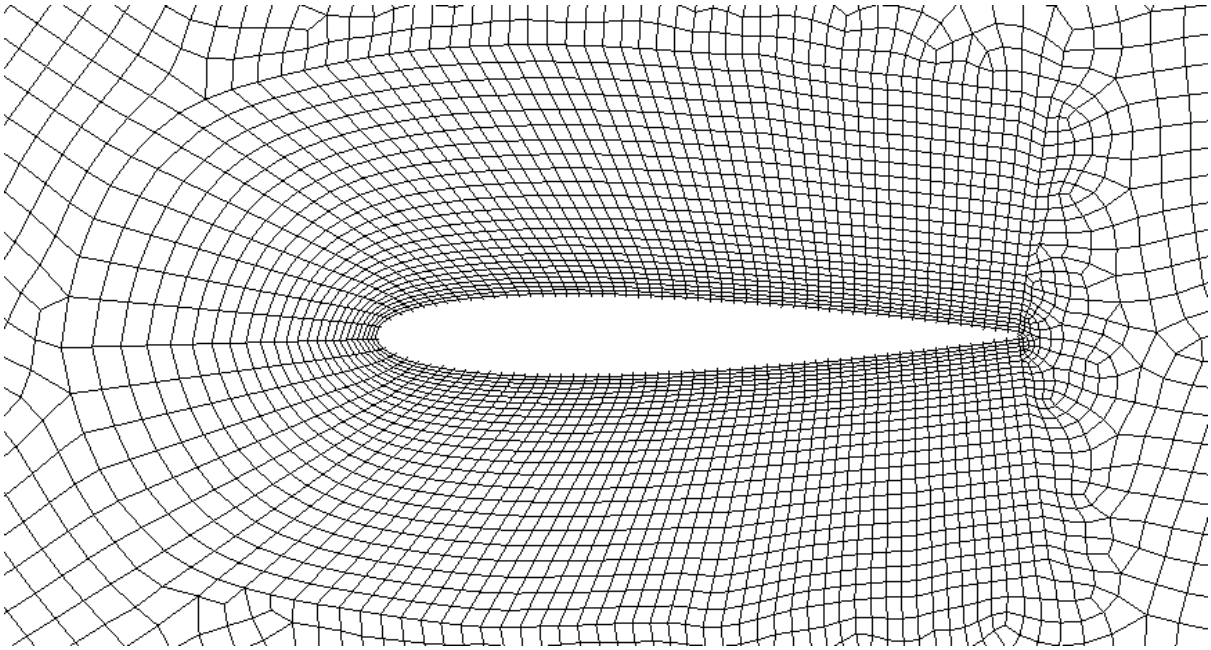

Figure 4-2 Inflation layers around the airfoil

Table 4-1 Parameters for mesh generation around airfoil

Mesh	Global Element size (mm)	Edge sizing	Inflation layers	First layer height (mm)	Growth rate	Face Sizing (mm)	Number of nodes	Aspect Ratio
1	6	80	15	0.1	1.2	1	12,037	6.07
2	5	100	25	0.05	1.1	0.5	22,124	4.34
3	4	140	35	0.025	1.05	0.25	47,254	6.68

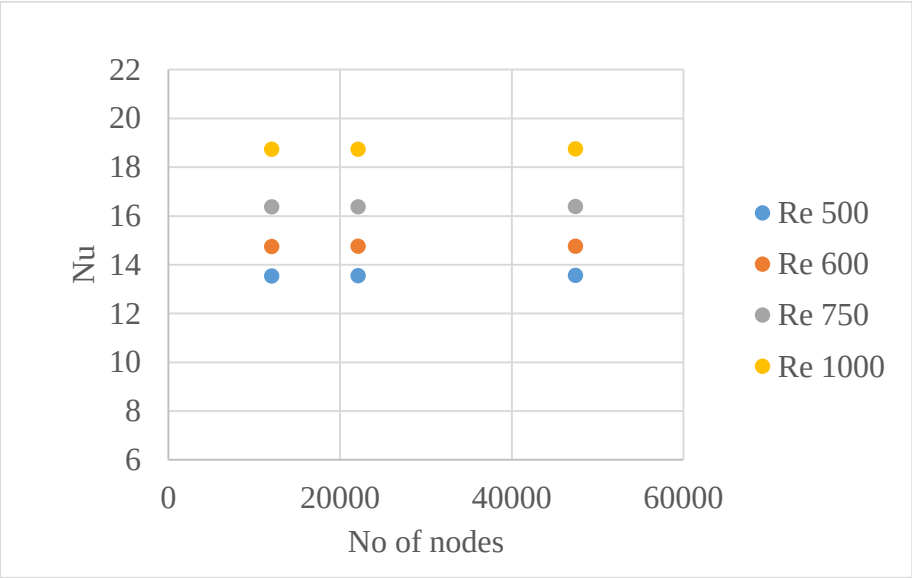

Figure 4-3 Mesh independence test

4.2 Heat transfer in two airfoils in adjacent and inline arrangement

Two NACA 0012 airfoils were kept in adjacent and inline arrangement as shown in Figure 4-4.

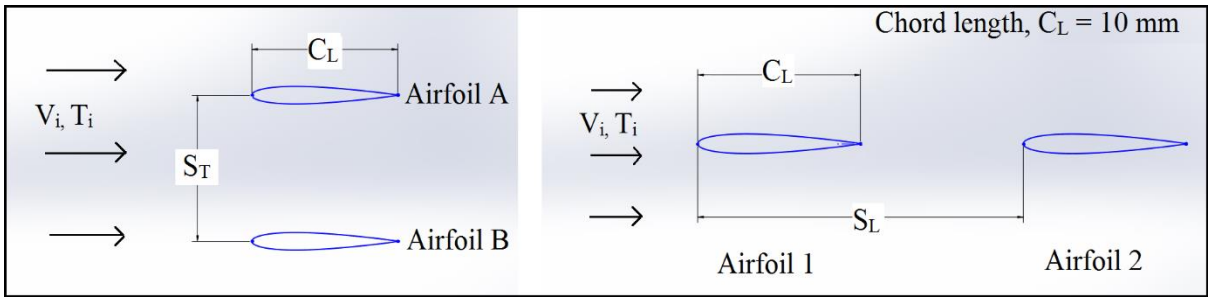

Figure 4-4 Two NACA airfoils in adjacent (left) and inline (right) configuration

In an adjacent configuration, the spanwise spacing, S_T, between the leading edge of airfoil-A and the leading edge of airfoil-B is varied, and the heat transfer from each airfoil is observed as shown in Figure 4-5. S_T is varied from 5mm to 60 mm. The Nusselt number was observed to be highest when the separation between the airfoils is at 5 mm. Similar to the cylindrical case, as in Section 3.2.2 , when the separation is increased, the Nusselt number decreases and reaches a steady value as expected.

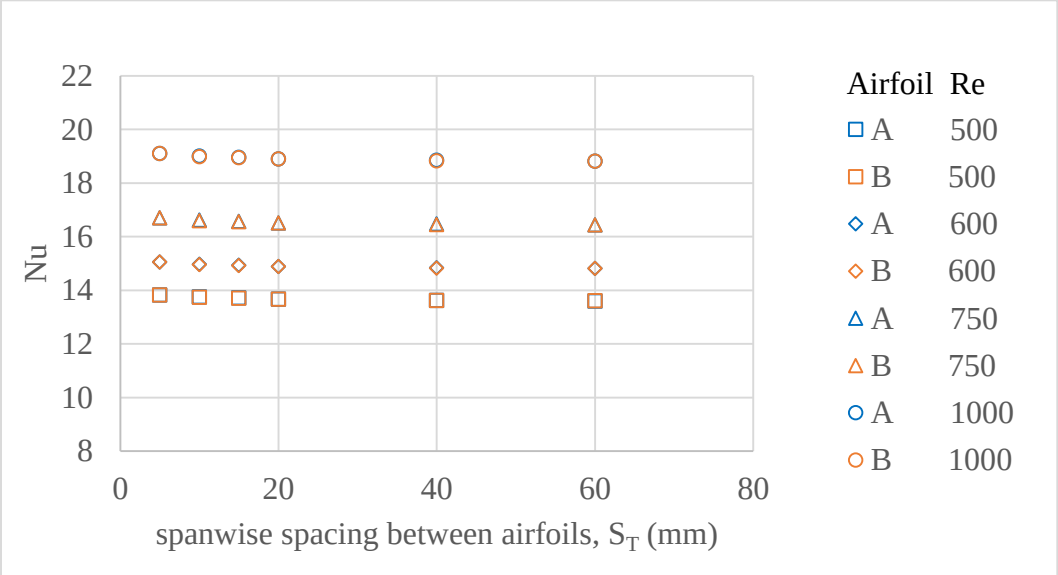

Figure 4-5 Nusselt number for airfoils in adjacent arrangement

In an inline arrangement, the streamwise separation, S_L, was taken from the leading edge of Airfoil-1 to the leading edge of Airfoil-2. The streamwise distance between the airfoils are varied from 1.5D to 8D, and the Nusselt number is compared, as shown in Figure 4-6. Similar to the cylindrical case (Section 3.2.2), the Nusselt number of airfoil-2 is observed to be far lower than airfoil-1 when the distance between them is small, and as the distance is increased, the Nusselt number also increased.

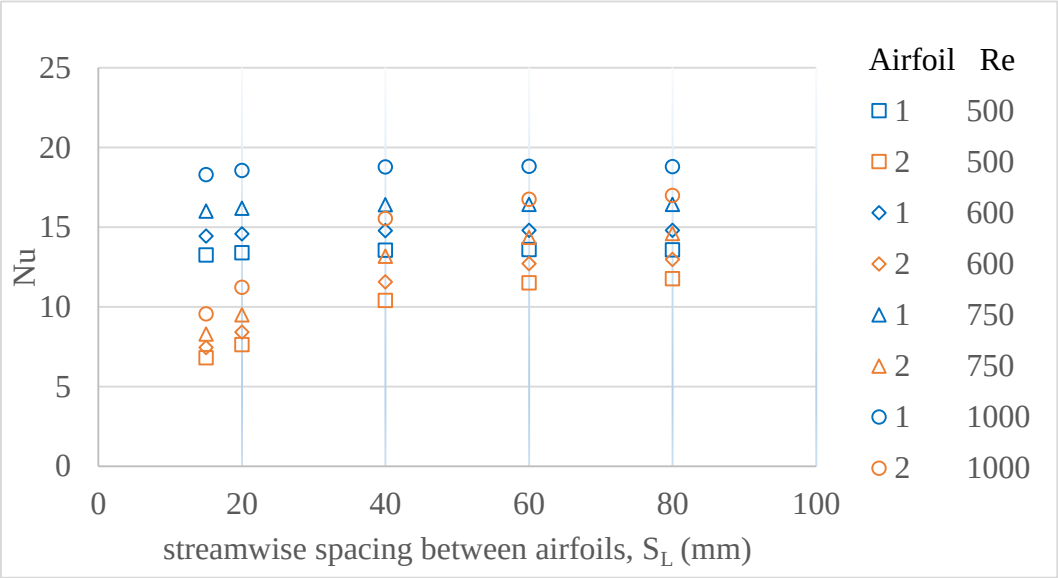

Figure 4-6 Nusselt number for airfoils in inline arrangement

4.3 Heat transfer from a 16-row array of airfoils

Simulation for heat transfer from 16-row airfoil array is done with periodic boundary conditions on the upper and lower edges, as shown in Figure 4-7. The chord length of the NACA 0012 airfoil used in the simulation is 10 mm. The streamwise pitch (S_L) and the spanwise pitch (S_T) between the airfoils are measured from the leading edge of one airfoil to

the leading edge of the second airfoil. A representative mesh of the airfoils is shown in Figure 4-8, which is generated using the mesh parameters selected in Section 4.1.2

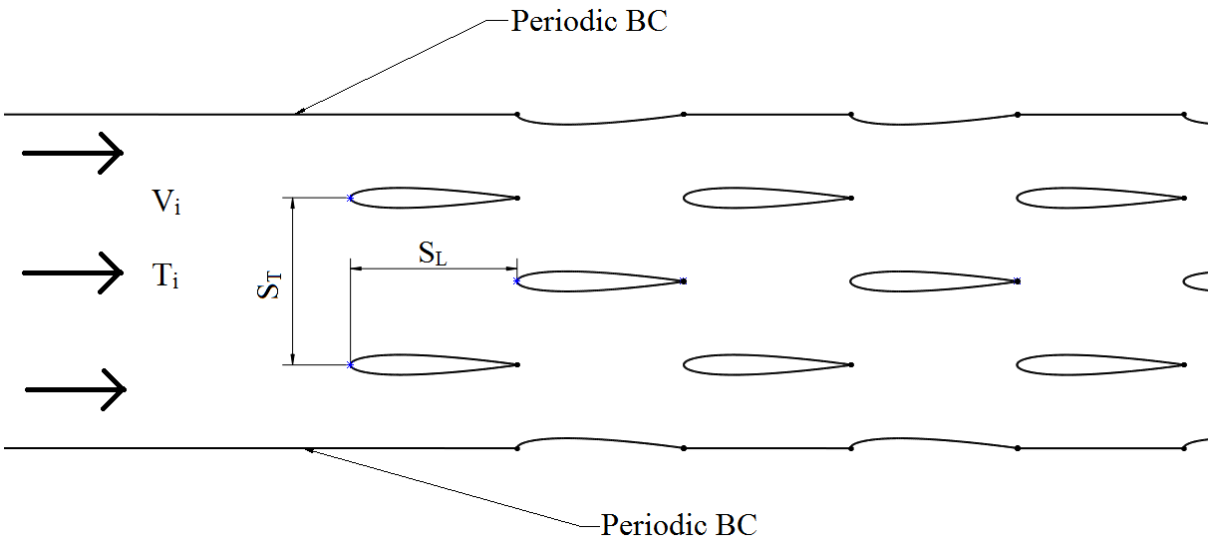

Figure 4-7 Domain for a staggered array of airfoils (0° AOA)

The mesh around the airfoils is generated using inflation layers, as shown in Figure 4-8.

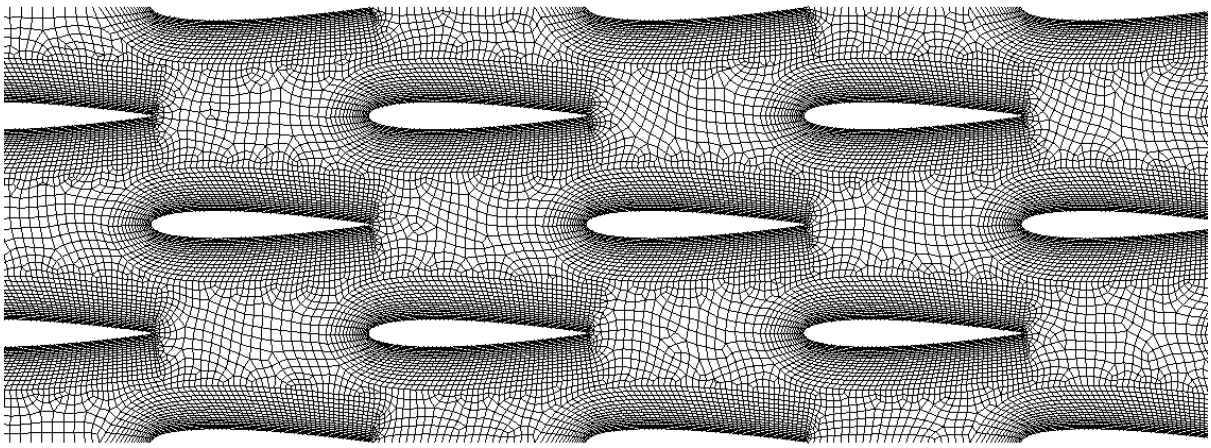

Figure 4-8 Generated mesh for airfoil array

The numerical simulation of staggered airfoils was done for three different angles of attack (0°, 5°, and 10°). As the angle of attack was changed, the airfoils were adjusted such that the whole

airfoils were encapsulated inside the domain while maintaining the spanwise spacing as shown in Figure 4-9.

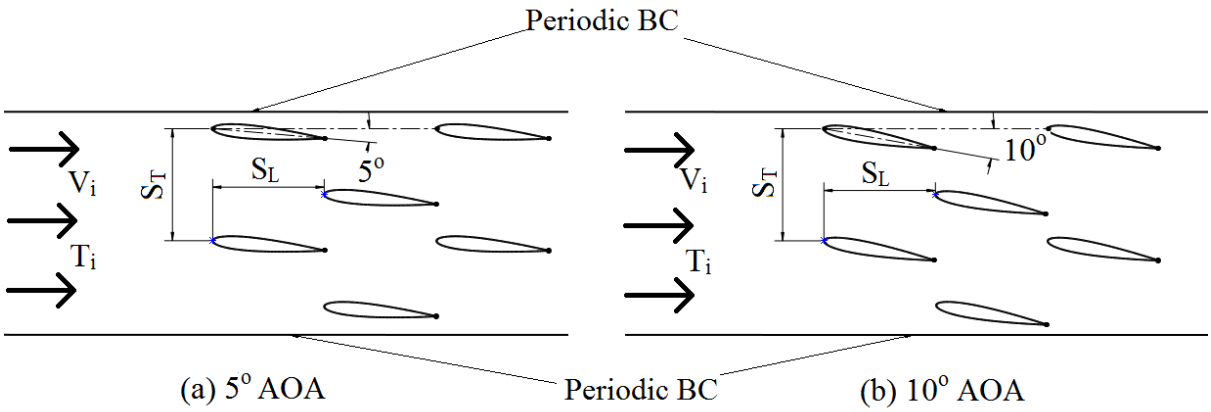

Figure 4-9 Airfoils at different angles of attack

For each angle of attack, nine different cases (similar to the cylindrical case) by varying the spanwise distance (S_T) and streamwise distance (S_L) were generated and run for simulation. Figure 4-10 shows the Nusselt number for a 0° angle of attack. The highest Nusselt number is found for the staggered arrangement of S_T = 1 C_L and S_L=1.5 C_L. It is also observed that when the streamwise spacing is kept constant, the Nusselt number is maximum for the smallest spanwise spacing and decreases as the spanwise spacing is increased. A similar trend can be seen from the results of the airfoil array with 5° AOA.

Figure 4-11 shows the Nusselt number for 5° angle of attack, and the highest Nusselt number is found for the staggered arrangement of S_T = 1 CL and S_L=1 CL. Figure 4-12 shows the Nusselt number for a 10° angle of attack, and the highest Nusselt number is found for the staggered arrangement of S_T = 1 CL and S_L=1 CL. Complete data results of Nusselt number for all angles of attacks can be found in Appendix Table B-1.

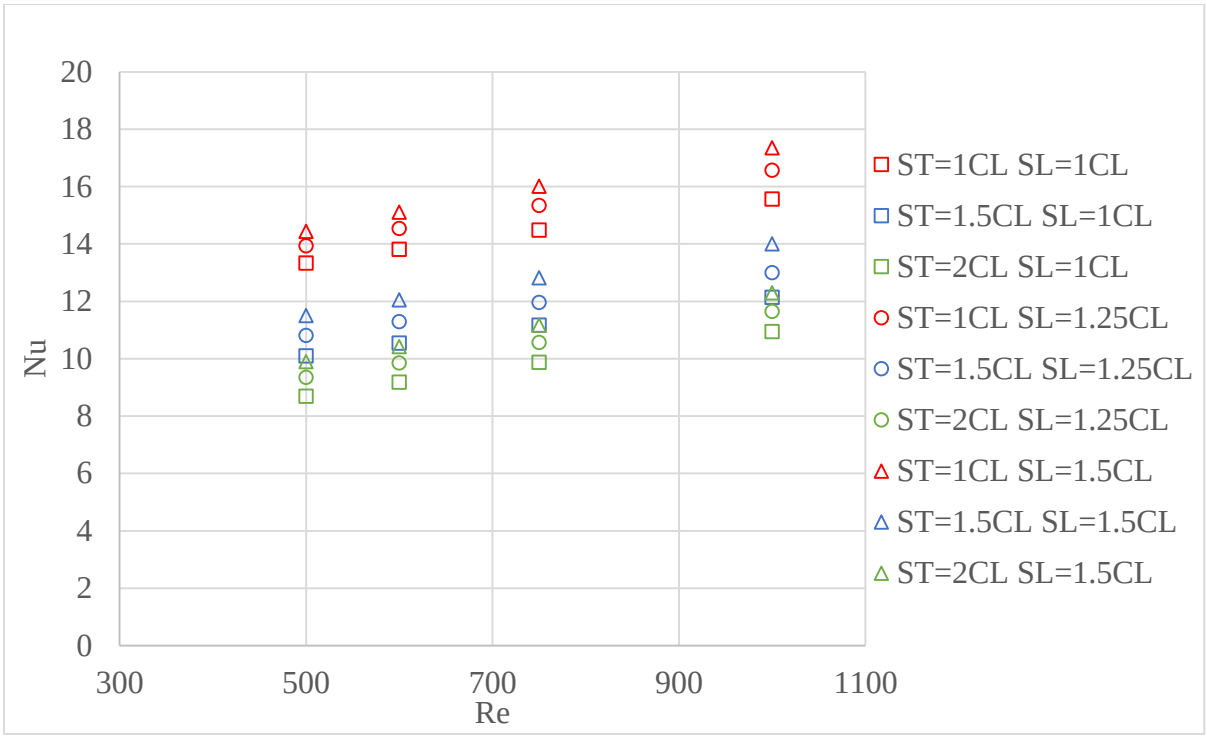

Figure 4-10 Nusselt number 16-row array of an airfoil with 0° angle of attack

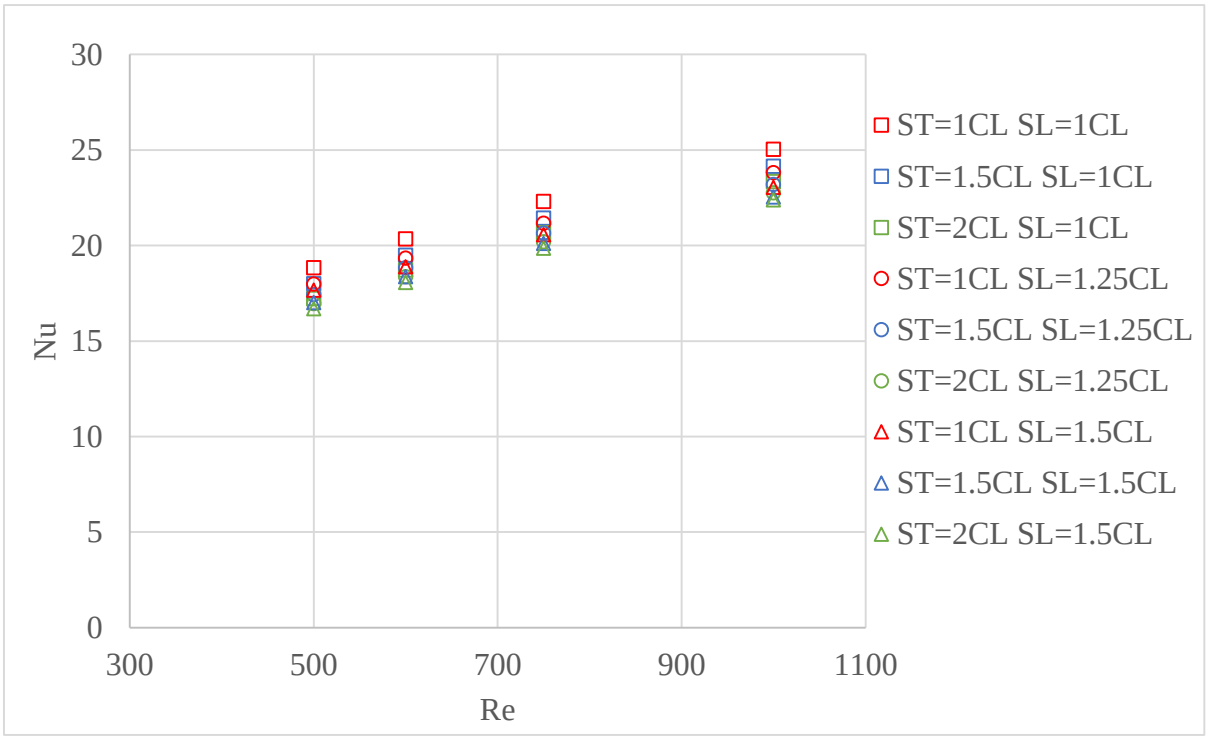

Figure 4-11 Nusselt number 16-row array of airfoil with 5° angle of attack

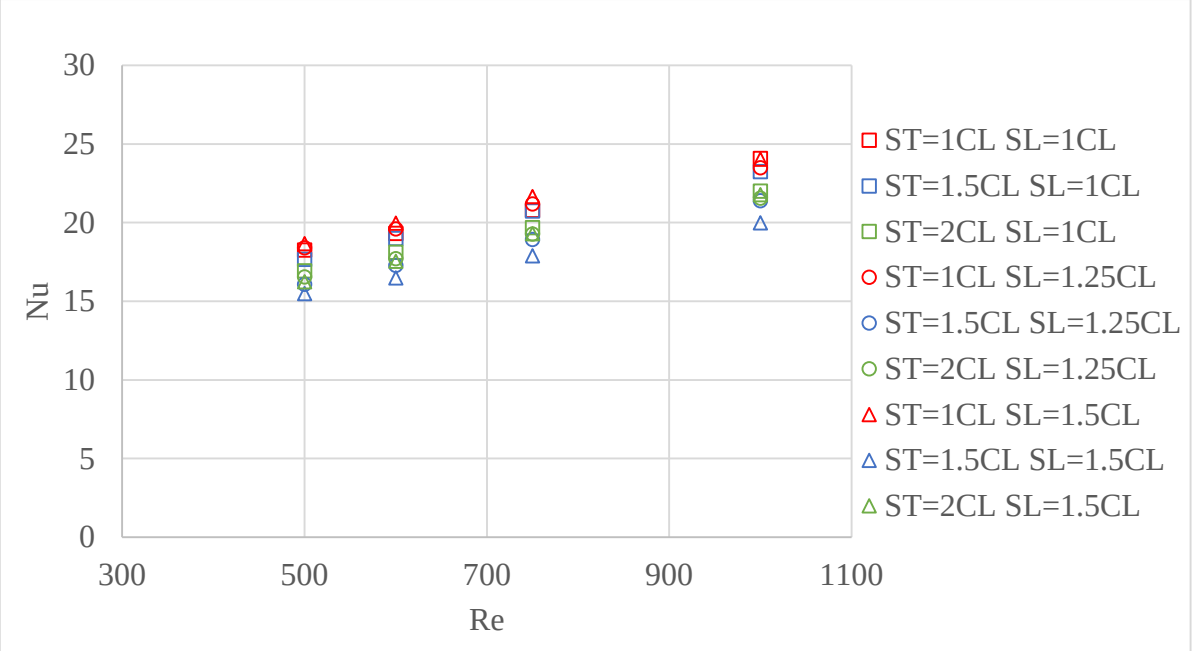

Figure 4-12 Nusselt number 16-row array of airfoil with 10° angle of attack

The comparison of arrangements of all three angles of attack with highest Nusselt number is shown in Figure 4-13, which shows that the Nusselt number is highest when the airfoils are kept at 5° angle of attack for spacings of S_T = 1 C_L and S_L=1 C_L.

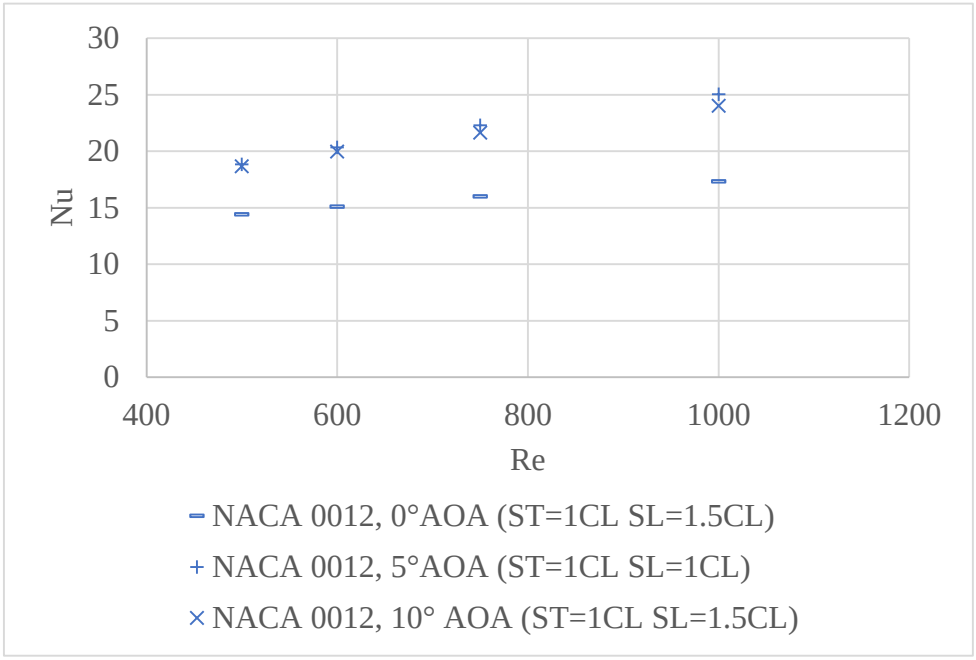

Figure 4-13 Highest Nu for all three angles of attack

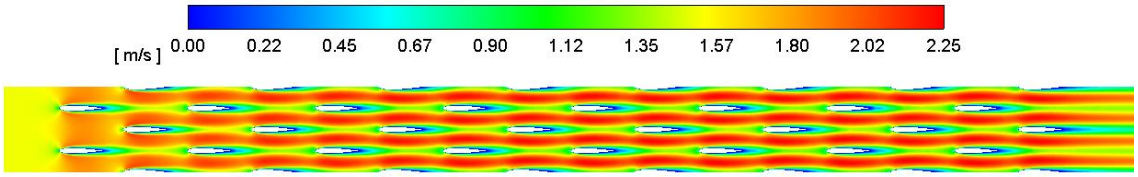

(a) S_T=1C_L, S_L=1.5C_L

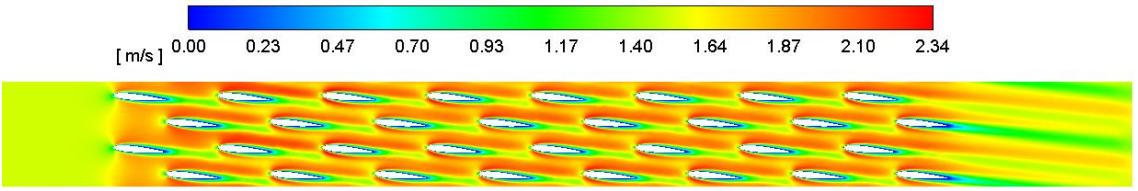

(b) S_T=1C_L, S_L=1C_L

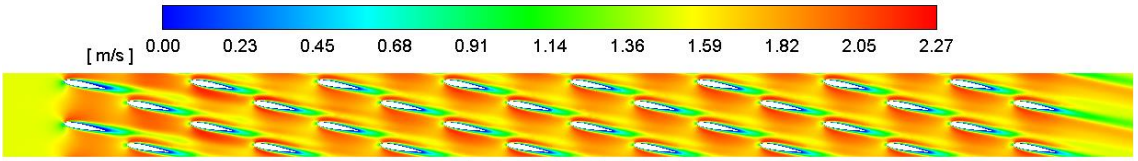

(c) S_T=1C_L, S_L=1.5C_L

Figure 4-14 Velocity contour for (a) 0° AOA, (b)5° AOA, and (c)10° AOA (Re 1000)

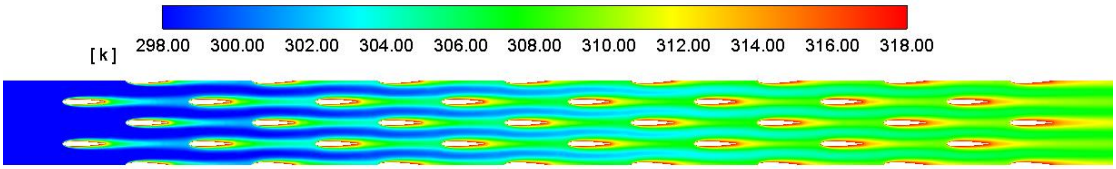

(a) S_T=1C_L, S_L=1.5C_L

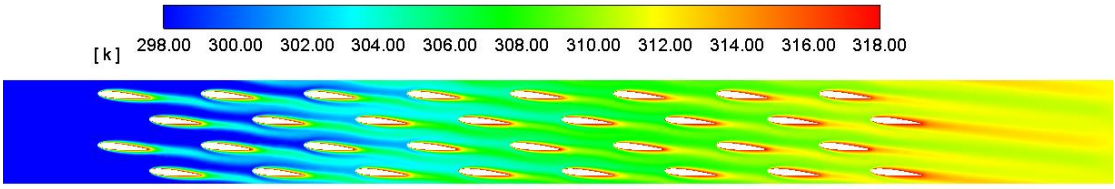

(b) S_T=1C_L, S_L=1C_L

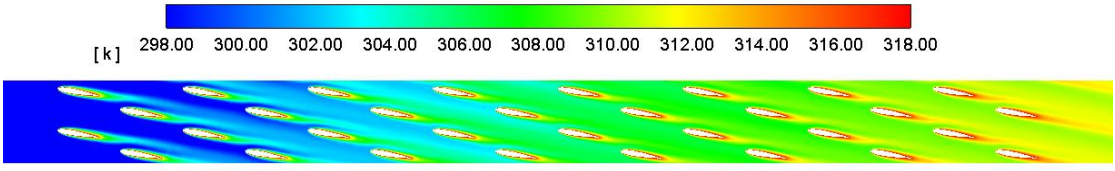

(c) S_T=1C_L, S_L=1.5C_L

Figure 4-15 Temperature contour for (a) 0° AOA, (b)5° AOA, and (c)10° AOA (Re 1000)

The velocity and temperature fields for all cases of Figure 4-13 are shown in Figure 4-14 and Figure 4-15. For 0°AOA, the outlet temperature is about 309 K. For 5° AOA and 10° AOA, the exit temperature of the fluid is about 312 K. The array with 5° AOA has a slight advantage with a higher Nusselt number and a smaller domain size.

Chapter 5 Results and Conclusion

5.1 Comparison between cylinder and NACA 0012 airfoil pin fins

Figure 5-1 shows the comparison of the Nusselt number for a single cylinder and a single airfoil case. It is observed that the Nusselt number for the airfoil case is higher than the cylinder case.

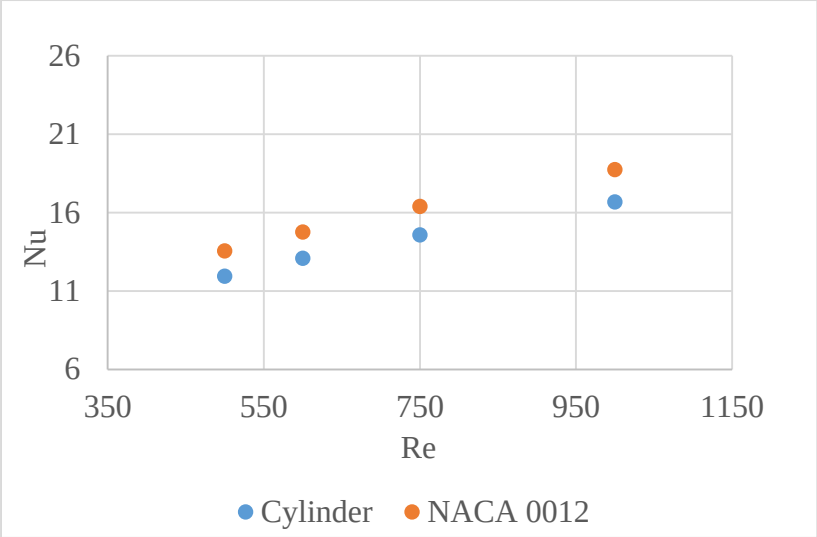

Figure 5-1 Nusselt number for a single cylinder and airfoil

From Section 0, among the nine different staggered arrangements of cylinders, the highest Nusselt number is obtained for a cylinder separation of S_T= 1.75D and S_L=1D. From Section 4.3. it is observed that among the different arrangement of NACA 0012 airfoil for all three angles of attack, the highest Nusselt number is obtained for a 5° angle of attack of the airfoils with the separation of airfoils of 1 chord length in both spanwise and streamwise direction (S_T= 1CL, S_L=1CL). The Nusselt number for the best case of cylinder array (S_T= 1.75D and S_L=1D) is found to be 1.3 to 1.4 times higher than the case of the airfoil array (S_T= 1CL, S_L=1CL) as shown in Figure 5-2. The Nusselt number is observed to be higher because of the geometrical shape of the cylindrical pin fins which enhances proper fluid mixing than the airfoil pin fins.

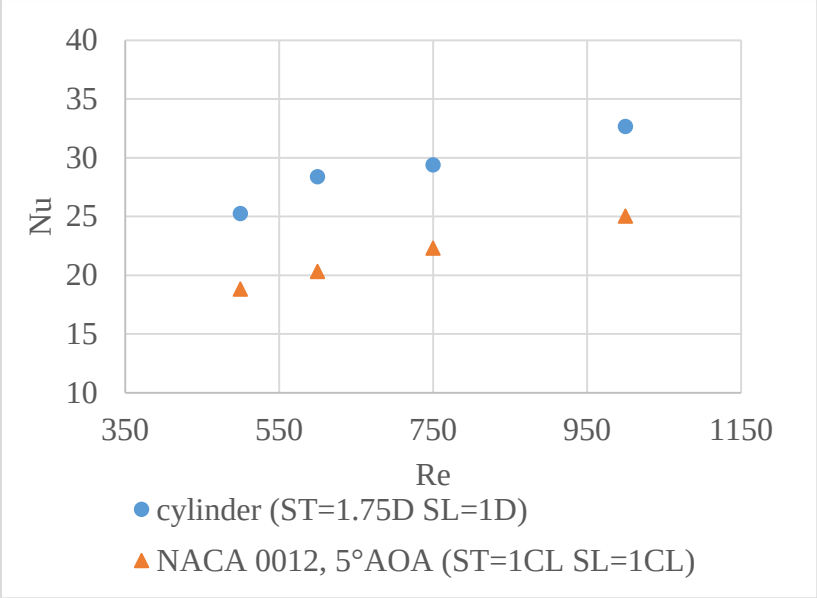

Figure 5-2 Nu for cylinder and NACA 0012 array

The heat transfer behavior alone does not provide a complete assessment of heat exchanger performance. The amount of the pressure drop also specifies the energy to maintain the required fluid flow for the heat transfer. Optimization of a heat sink considers the change in pressure while improving the heat transfer. Thus, a change in pressure drop should be weighed against the change in heat transfer behavior while selecting a pin finned heat sink. In this study, the pressure drop of a heat sink is calculated by the difference in the fluid's total pressure in the inlet section and the fluid's total pressure in the outlet section. The total pressure was directly extracted from ANSYS Fluent as an averaged value over the domain cross-section.

The staggered arrangement of the cylinders has a better advantage in terms of heat transfer. This result agrees with the research of Sahiti [3], where it is pointed out that for low Reynolds number (Re<1000), Nusselt number in airfoil arrangement is lower than the cylindrical case. They also concluded that the pressure drop in cylindrical is higher than airfoil array, which is similar to this study as shown in Figure 5-3, where the pressure drop in cylinder array is 14-25 times higher than airfoil array.

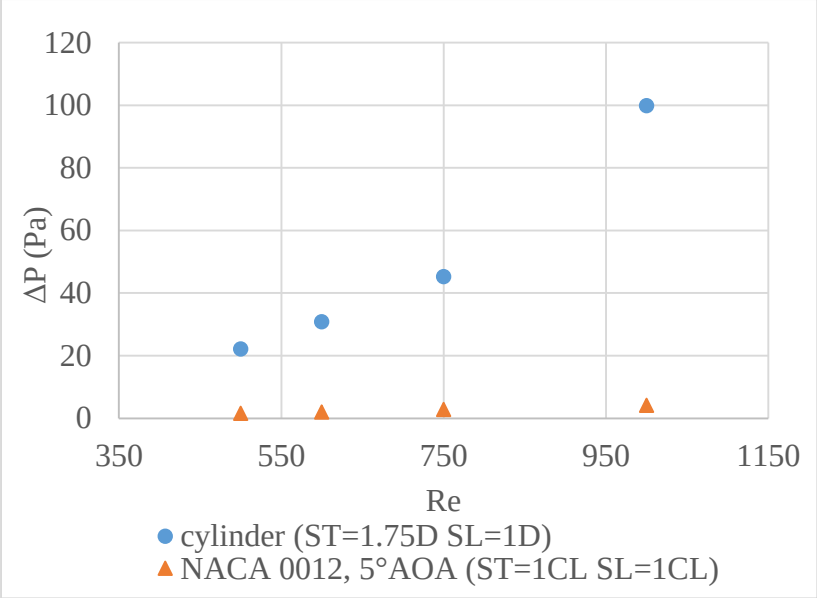

Figure 5-3 Pressure difference for cylinder and NACA 0012 array

Further simulation was carried by decreasing the airfoil spanwise spacing to 0.5 times the chord length (0.5 C_L) while keeping the streamwise spacing equal to a chord length (1C_L). The domain width decreased to 10 mm. The Nusselt number for this arrangement was observed to be much closer to the best case of cylinder array, as shown in Figure 5-4. The Nusselt number for cylinder array was about 1.1 times higher than that of airfoil array with a maximum difference of 3.75. However, as the spacing is decreased in the airfoil array, the pressure drop also slightly increased but was still significantly less than that of the cylinder array as shown in Figure 5-5. The pressure drop is observed to be 5-9 times higher in the cylinder array compared to that of the airfoil array with a maximum difference of 88.12 Pa at Re =1000.

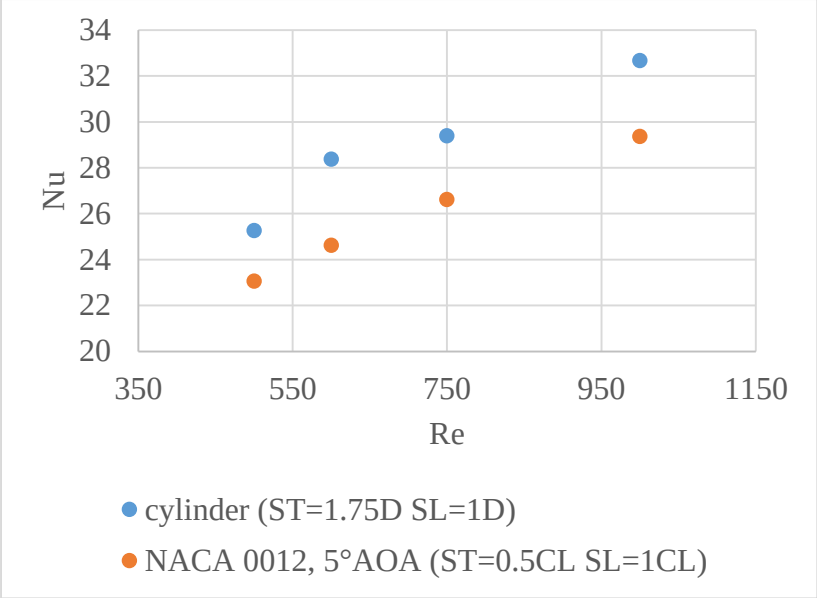

Figure 5-4 Nu for reduced spanwise spacing of airfoil

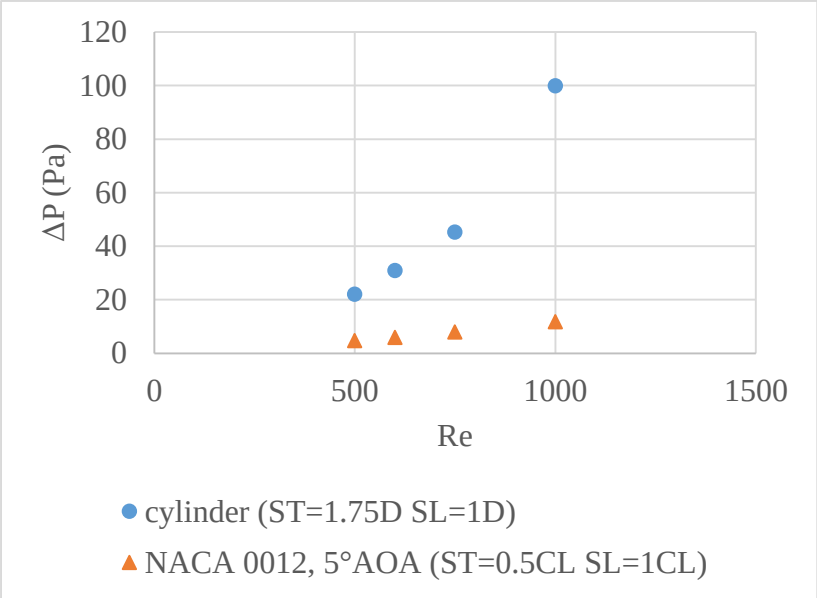

Figure 5-5 Pressure difference for reduced spanwise spacing of airfoil

A larger Nusselt number corresponds to a more effective convective heat transfer, but does not reflect the system's overall heat transfer rate. But, the arrangement of cylinders and airfoils in an array in this study has a different domain width based on the fins spanwise spacing. This is

because of the use of periodic boundary conditions on the domain's top and bottom horizontal planes. The best case of cylinder array (S_T=1.75D, S_L=1D) has a domain width of 3D, while the airfoil array (S_T=0.5CL, S_L=1CL) has a domain width equal to 1C_L. In order to have the same heat transfer base area, the domain size of both arrays should be the same to check the overall heat transfer rate from the system. Simulation of airfoil array (S_T=0.5CL, S_L=1CL) was carried out in the same domain width as cylinder case, i.e., at 3.5D. This domain confined a total of 112 airfoils, while for cylinder (S_T=1.75CL, S_L=1CL), the domain confined only 32 cylinders. Since the arrangement of the airfoils is still the same, the Nusselt number and the pressure drop of the array was found to be the same as in Figure 5-4 and Figure 5-5. Since the surface area for heat transfer drastically increased for the airfoil array, which is about 2.5 times that of the cylinder array, the rate of heat transfer also increased as shown in Figure 5-6. The overall heat transfer rate in the airfoil array is about 1.2 times higher than that of the cylinder array with a maximum difference of 247 W/m at Re=1000 for the same domain size.

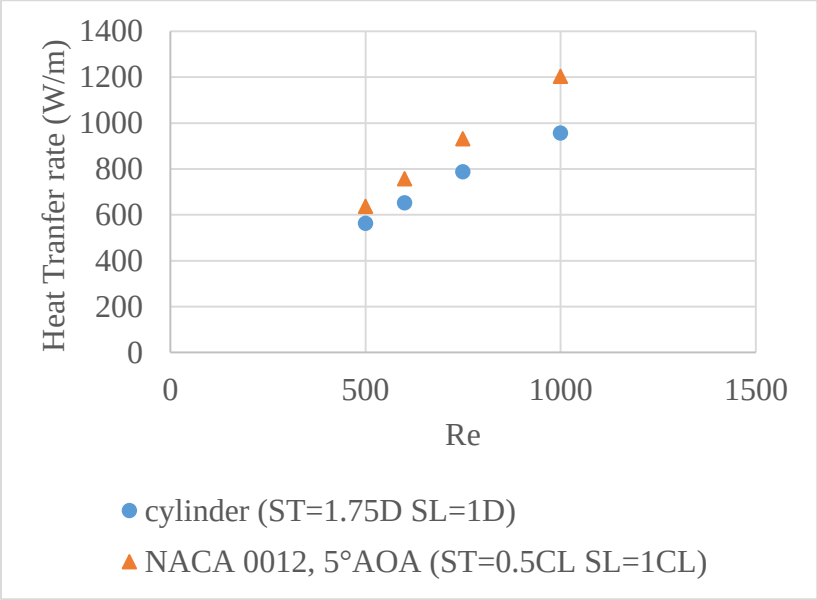

Figure 5-6 Overall heat transfer rate for same domain width

Furthermore, the airfoils' arrangement was adjusted in a meandering arrangement to observe the heat transfer behavior. The airfoils were kept at a 5° angle of attack in the first row, at a 0° angle of attack in the second row, at a -5° angle of attack in the third row, and at a 0° angle of attack in the fourth row. The process was repeated until the 16th row. The arrangement is shown in Figure 5-7.

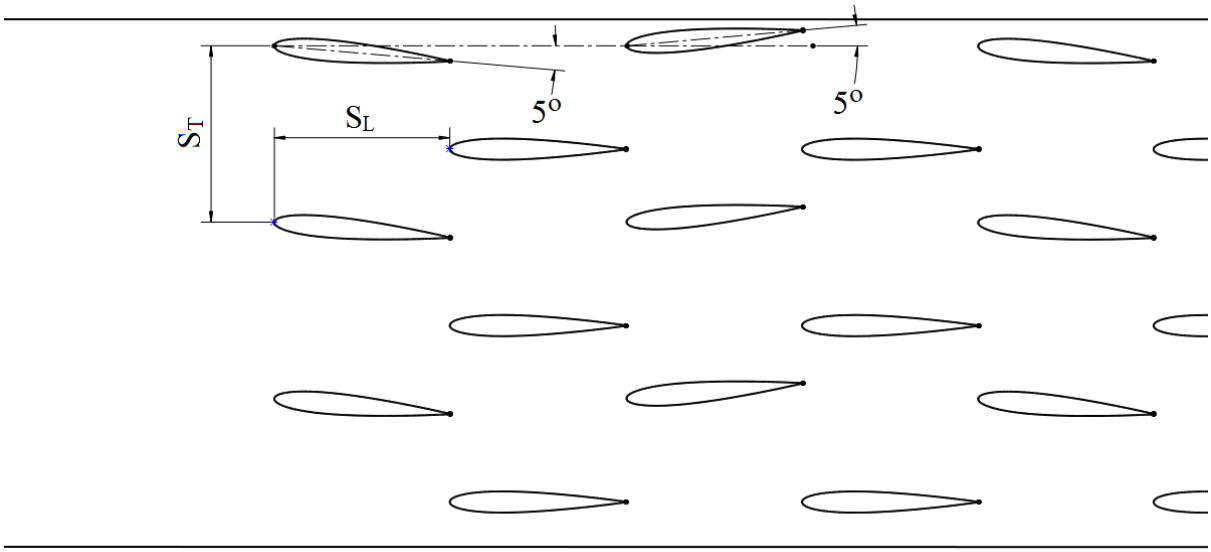

Figure 5-7 Meandering arrangement of airfoils

The domain size is the same as the previous simulation of 35 mm, and thus contains 112 airfoils. The heat transfer and the pressure drop from the arrangement is observed to be very close to that of the airfoil at 5° angle of attack in a staggered position, as shown in the Figure 5-8 and Figure 5-9. The temperature and velocity contours for airfoil array at 5° AOA (S_T=0.5C_L) and meandering arrangement are shown in Figure 5-10 and Figure 5-11. It is observed that the temperature of the fluid is similar in both cases as they pass through the pin fin rows.

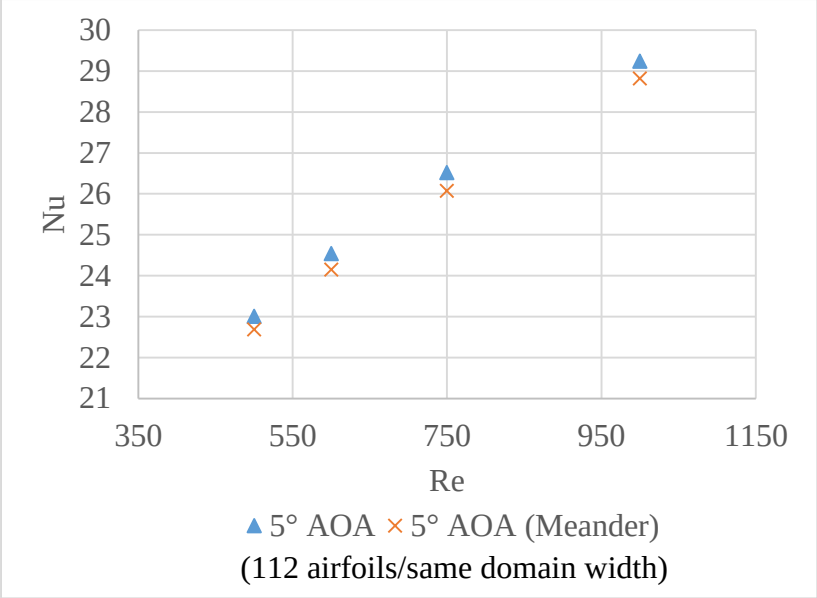

Figure 5-8 Nu for meandering airfoils

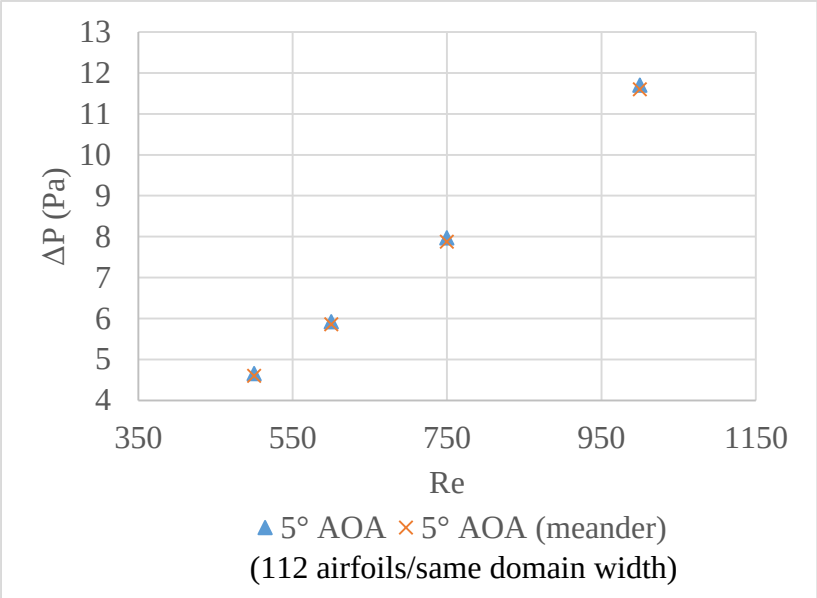

Figure 5-9 Pressure drop for meandering airfoils

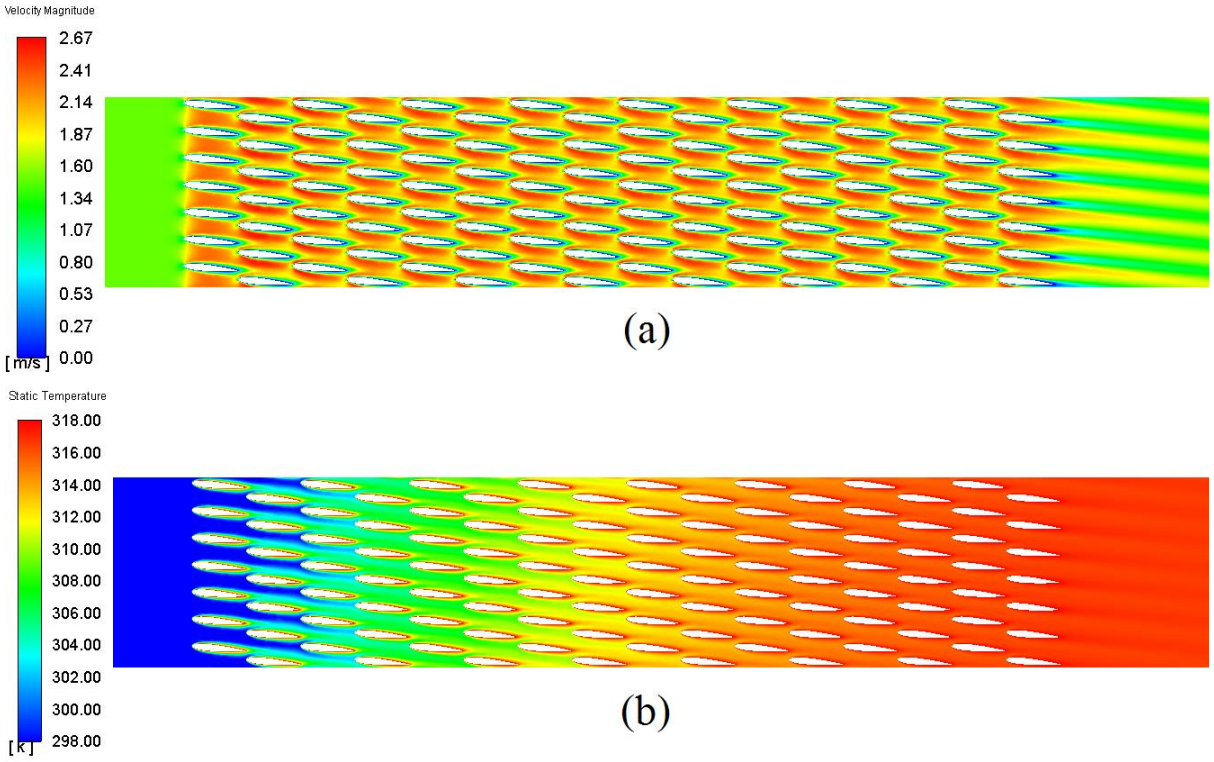

Figure 5-10 5° AOA (a) Velocity contour (b) Temperature contour (Re=1000)

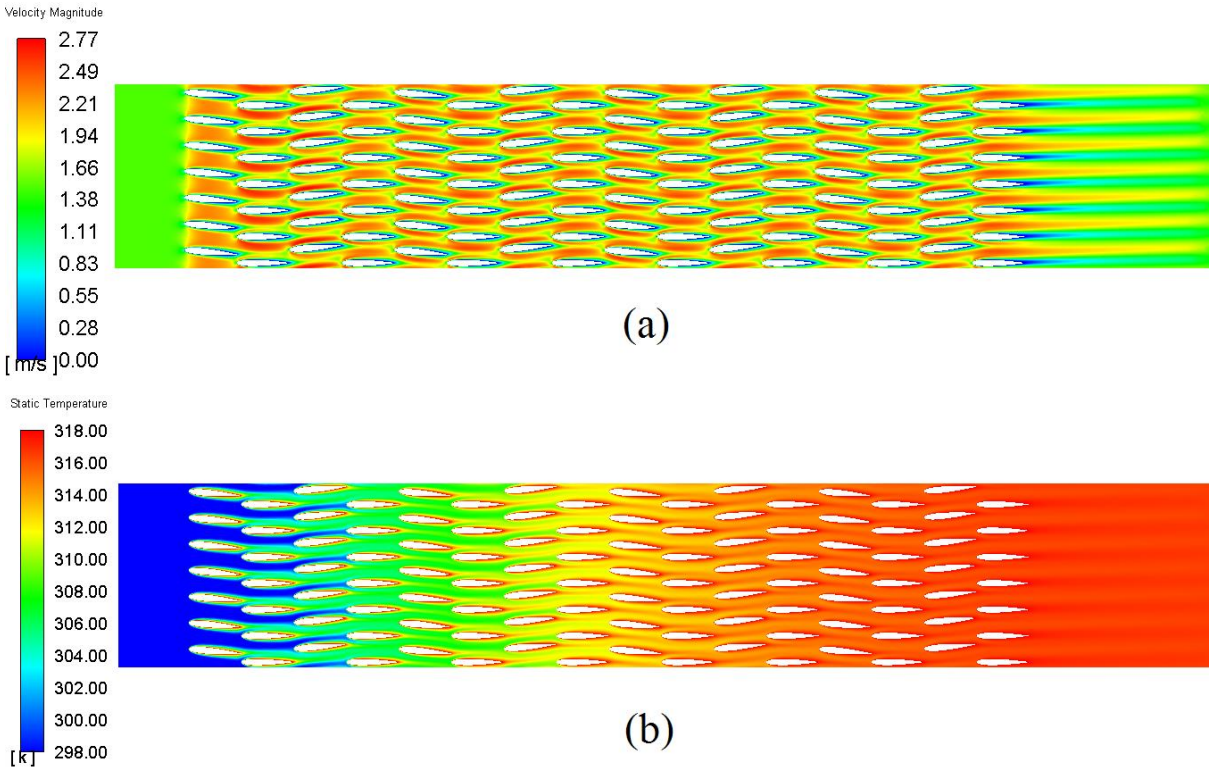

Figure 5-11 Meandering airfoils (a) Velocity contour (b) Temperature contour (Re=1000)

5.2 Conclusion

Numerical simulation has been performed, starting from a single cylinder to 16-row array cylinders arranged in a staggered pattern. These models have been compared with the established empirical correlations and were in good agreement. Using 16-row staggered array, different configurations based on spanwise and streamwise spacing have been simulated to find the arrangement with the best heat transfer performance. It is observed for the configuration, S_T = 1.75D and S_L = 1D, the Nusselt number is higher compared to other cylindrical arrays.

Following a similar approach as cylinders, a study has been performed in 16-row array NACA 0012 airfoil arranged in a staggered pattern for nine different configurations at three different angles of attack (0°, 5°, and 10°). The highest Nusselt number was obtained for a 5° angle of attack with the configuration $S_T = 0.5C_L$ and $S_L = 1C_L$, which is the best case of airfoils in a staggered arrangement in this study.

Even though Nusselt number of the best cylindrical array is about 1.1 times higher than the best airfoil case, the airfoil array's overall heat transfer rate was 1.2 times higher than that of the cylinder array. This is because more airfoils can be packed in the same domain size, which increases the overall heat transfer while keeping the pressure drop significantly lower than that of cylinders. This shows that the staggered airfoils at 5^0 angle of attack with the configuration $S_T = 0.5C_L$ and $S_L = 1C_L$ is better than the cylindrical arrangements for Re<1000.

A case of meandering arrangement of the airfoils was compared with the best case of staggered airfoil array, and was found that the heat transfer and the pressure drop were very similar.

For a practical purpose of electronic cooling, factors such as the cost of manufacturing a pin fin heat sink and the power consumption for cooling the heat sink comes into consideration

while selecting the type of pin finned heat sink. In conclusion, it can be said that airfoil array at 5° angle of attack is favorable as it has a considerably satisfying Nusselt number with a better overall heat transfer rate than a cylindrical array. Moreover, NACA airfoil array has better performance in heat transfer without any drastic pressure loss, which reduces the power consumption for pumping fluid compared to that of a cylindrical array and is just as easy to fabricate using additive manufacturing.

5.3 Recommendation for future work

- Perform time-dependent study to determine unsteady flow characteristics for airfoil arrays
- Various cases could be studied for more angle of attacks of the airfoil and spacing between the fins.
- Heat transfer study from cambered NACA airfoil.
- Experimental work to validate the numerical study.
- Use of additive manufacturing of heat sink with different arrangements of airfoil pin fins.

References

[1] S. S. Anandan and V. Ramalingam, “Thermal management of electronics: A review of literature,” *Therm. Sci.*, vol. 12, no. 2, pp. 5–25, 2008, doi: 10.2298/TSCI0802005A.

[2] E. M. Sparrow, J. W. Ramsey, and C. A. C. Altemani, “Experiments on In-line Pin Fin Arrays-and Performance Comparisons with Staggered Arrays,” vol. 102, no. February 1980, pp. 44–50, 1980.

[3] N. Sahiti, A. Lemouedda, D. Stojkovic, F. Durst, and E. Franz, “Performance comparison of pin fin in-duct flow arrays with various pin cross-sections,” *Appl. Therm. Eng.*, vol. 26, no. 11–12, pp. 1176–1192, 2006, doi: 10.1016/j.applthermaleng.2005.10.042.

[4] D. P. D. Theodore L. Bergman, Adrienne S. Lavine, Frank P. Incropera, *Fundamentals of Heat and Mass Transfer, 8th Edition | Wiley*. 2017.

[5] K. Bilen, U. Akyol, and S. Yapici, “Heat transfer and friction correlations and thermal performance analysis for a finned surface,” *Energy Convers. Manag.*, vol. 42, no. 9, pp. 1071–1083, 2001, doi: 10.1016/S0196-8904(00)00119-9.

[6] A. Žkauskas, “Heat Transfer from Tubes in Crossflow,” *Adv. Heat Transf.*, vol. 18, no. C, pp. 87–159, 1987, doi: 10.1016/S0065-2717(08)70118-7.

[7] B. Adrian, *CONVECTION HEAT Other books by Adrian Bejan :* 2013.

[8] A. Bejan, “The Optimal Spacing for Cylinders in Crossflow Forced Convection,” *J. Heat Transfer*, vol. 117, no. 3, p. 767, 2008, doi: 10.1115/1.2822645.

[9] B. A. Jubran, M. A. Hamdan, and R. M. Abdualh, “Enhanced Heat Transfer, Missing

Pin, and Optimization for Cylindrical Pin Fin Arrays," *J. Heat Transfer*, vol. 115, no. 3, p. 576, 2008, doi: 10.1115/1.2910727.

[10] W. A. Khan, J. R. Culham, and M. M. Yovanovich, "Modeling of cylindrical pin-fin heat sinks for electronic packaging," *IEEE Trans. Components Packag. Technol.*, vol. 31, no. 3, pp. 536–545, 2008, doi: 10.1109/TCAPT.2008.2002554.

[11] I. Tokura, H. Saito, K. Kishinami, and K. Muramoto, "An Experimental Study of Free Convection Heat Transfer From a Horizontal Cylinder in a Vertical Array Set in Free Space Between Parallel Walls," *J. Heat Transfer*, vol. 105, no. 1, p. 102, 2009, doi: 10.1115/1.3245526.

[12] O. Terukazu, N. Hideya, and T. Yukiyasu, "Heat transfer and flow around an elliptic cylinder," *Int. J. Heat Mass Transf.*, vol. 27, no. 10, pp. 1771–1779, 1984, doi: 10.1016/0017-9310(84)90159-5.

[13] Q. Li, Z. Chen, U. Flechtner, and H. J. Warnecke, "Heat transfer and pressure drop characteristics in rectangular channels with elliptic pin fins," *Int. J. Heat Fluid Flow*, vol. 19, no. 3, pp. 245–250, 1998, doi: 10.1016/S0142-727X(98)00003-4.

[14] Z. Chen, Q. Li, D. Meier, and H. J. Warnecke, "Convective heat transfer and pressure loss in rectangular ducts with drop-shaped pin fins," *Heat Mass Transf. und Stoffuebertragung*, vol. 33, no. 3, pp. 219–224, 1997, doi: 10.1007/s002310050181.

[15] O. Uzol and C. Camci, "Heat Transfer, Pressure Loss and Flow Field Measurements Downstream of Staggered Two-Row Circular and Elliptical Pin Fin Arrays," *J. Heat Transfer*, vol. 127, no. 5, p. 458, 2005, doi: 10.1115/1.1860563.

[16] F. Wang, J. Zhang, and S. Wang, "Investigation on flow and heat transfer characteristics

in rectangular channel with drop-shaped pin fins," *Propuls. Power Res.*, vol. 1, no. 1, pp. 64–70, 2012, doi: 10.1016/j.jppr.2012.10.003.

[17] F. Zhou and I. Catton, "Numerical Heat Transfer , Part A : Applications An International Journal of Computation and Methodology Numerical Evaluation of Flow and Heat Transfer in Plate-Pin Fin Heat Sinks with Various Pin Cross- Sections," vol. 7782, 2011, doi: 10.1080/10407782.2011.588574.

[18] H. M. Jaffal, H. S. Jebur, and A. A. Hussein, "Numerical and Experimental Investigations on the Performance Characteristics for Different Shapes Pin Fin Heat Sink," vol. 4, no. 3, pp. 330–343, 2018.

[19] X. Wang, E. Bibeau, and G. F. Naterer, "Experimental correlation of forced convection heat transfer from a NACA airfoil," *Exp. Therm. Fluid Sci.*, vol. 31, no. 8, pp. 1073–1082, 2007, doi: 10.1016/j.expthermflusci.2006.11.008.

[20] J. Y. Ho, K. K. Wong, K. C. Leong, and T. N. Wong, "Convective heat transfer performance of airfoil heat sinks fabricated by selective laser melting," *Int. J. Therm. Sci.*, vol. 114, pp. 213–228, 2017, doi: 10.1016/j.ijthermalsci.2016.12.016.

[21] M. E. C. William M. Kays, "Convective Heat and Mass Transfer." 1993, doi: 10.1007/978-1-4419-1564-1_7.

[22] K. Yousefi and A. Razeghi, "Determination of the Critical Reynolds Number for Flow," no. January, pp. 1–11, 2018, doi: 10.2514/6.2018-0818.

Appendix A

Table A- 1 Nusselt number for single cylinder in crossflow

Re	Nu (Hilpert)	Nu (simulation)	% Difference
500	11.02	11.94	8.37
600	11.99	13.07	8.97
750	13.31	14.56	9.43
1000	15.22	16.67	9.52

Table A- 2 Nusselt number for staggered arrangement of cylinders

Arrangement	Re	Nu (Zukauskas)	Nu (Simulation)	% Difference
S_T=1.75D S_L=1D (domain width = 35 mm)	500	23.61	25.27	7.02
	600	26.34	28.38	7.73
	750	30.11	29.40	2.36
	1000	35.78	32.67	8.69
S_T=2D S_L=1D	500	22.12	23.81	7.64
	600	24.68	26.94	9.15

(domain width = 40 mm)	750	28.22	29.58	4.82
	1000	33.53	32.96	1.71
S_T=2.25D S_L=1D (domain width = 45 mm)	500	21.26	21.79	2.47
	600	23.73	24.58	3.60
	750	27.12	27.09	0.11
	1000	32.23	31.47	2.37
S_T=1.75D S_L=1.25D (domain width = 35 mm)	500	22.58	20.08	11.08
	600	25.19	22.37	11.19
	750	28.79	24.86	13.65
	1000	34.22	28.72	16.06
S_T=2D S_L=1.25D (domain width = 40 mm)	500	22.58	20.08	11.08
	600	25.19	22.37	11.19
	750	28.79	24.86	13.65
	1000	34.22	28.72	16.06
S_T=2.25D S_L=1.25D	500	20.33	19.43	4.46
	600	22.69	21.79	3.98

(domain width = 45 mm)	750	25.94	24.55	5.33
	1000	30.82	27.91	9.44
S_T=1.75D S_L=1.5D (domain width = 35 mm)	500	21.77	19.56	10.17
	600	24.29	22.20	8.60
	750	27.76	24.67	11.15
	1000	32.99	28.57	13.41
S_T=2D S_L=1.5D (domain width = 40 mm)	500	20.40	18.10	11.30
	600	22.76	20.52	9.85
	750	26.02	22.70	12.75
	1000	30.92	26.65	13.83
S_T=2.25D S_L=1.5D (domain width = 45 mm)	500	19.61	18.16	7.36
	600	21.88	20.26	7.38
	750	25.01	22.48	10.12
	1000	29.72	26.31	11.47

Appendix B

Table B-1 Nusselt number for staggered airfoils for all angle of attacks

Arrangement	Re	Nu		
		0° AOA	5° AOA	10° AOA
S_T=1 C_L S_L=1 C_L (domain width = 20 mm)	500	13.34	18.84	18.25
	600	13.82	20.33	19.32
	750	14.49	22.30	20.78
	1000	15.56	25.04	24.08
S_T=1.5 C_L S_L=1 C_L (domain width = 30 mm)	500	10.10	17.99	17.67
	600	10.54	19.48	18.99
	750	11.17	21.43	20.74
	1000	12.14	24.14	23.24
S_T=2 C_L S_L=1 C_L (domain width = 40 mm)	500	8.69	17.23	16.94
	600	9.18	18.72	18.11
	750	9.88	20.65	19.69
	1000	10.95	23.35	22.00
S_T=1 C_L	500	13.94	17.97	18.41

S_L=1.25 C_L (domain width = 20 mm)	600	14.54	19.33	19.59
	750	15.35	21.16	21.18
	1000	16.57	23.80	23.49
S_T=1.5 C_L S_L=1.25 C_L (domain width = 30 mm)	500	10.82	17.43	16.07
	600	11.29	18.82	17.28
	750	11.96	20.64	18.93
	1000	13.00	23.19	21.39
S_T=2 C_L S_L=1.25 C_L (domain width = 40 mm)	500	9.35	16.95	16.54
	600	9.86	18.36	17.71
	750	10.57	20.19	19.28
	1000	11.65	22.75	21.56
S_T=1 C_L S_L=1.5 C_L (domain width = 20 mm)	500	14.44	17.66	18.67
	600	15.11	18.88	19.97
	750	16.01	20.55	21.66
	1000	17.35	23.03	24.03
S_T=1.5 C_L S_L=1.5 C_L	500	11.50	17.01	15.48
	600	12.05	18.36	16.49

(domain width = 30 mm)	750	12.82	20.10	17.89
	1000	14.00	22.54	19.98
$S_T=2\ C_L\ S_l=1.5\ C_L$ (domain width = 40 mm)	500	9.90	16.68	16.24
	600	10.43	18.06	17.55
	750	11.17	19.86	19.29
	1000	12.29	22.38	21.78